Article

Designing allosteric modulators to change GPCR G protein subtype selectivity

https://doi.org/10.1038/s41586-025-09643-2

Received: 17 November 2024

Accepted: 17 September 2025

Published online: 22 October 2025

Open access

Check for updates

Madelyn N. Moore[1,6], Kelsey L. Person[1,6], Valeria L. Robleto[1], Abigail R. Alwin[1], Campbell L. Krusemark[1], Noah Foster[1], Caroline Ray[2], Asuka Inoue[3,4], Michael R. Jackson[5], Michael J. Sheedlo[1], Lawrence S. Barak[2], Ezequiel Marron Fernandez de Velasco[1], Steven H. Olson[5] & Lauren M. Slosky[1]✉

G-protein-coupled receptors (GPCRs) convert extracellular signals into intracellular responses by signalling through 16 subtypes of Gα proteins and two β-arrestin proteins. Biased compounds—molecules that preferentially activate a subset of these proteins—engage therapy-relevant pathways more selectively[1] and promise to be safer, more effective medications than compounds that uniformly activate all pathways[2]. However, the determinants of bias are poorly understood, and we lack rationally designed molecules that select for specific G proteins. Here, using the prototypical class A GPCR neurotensin receptor 1 (NTSR1), we show that small molecules that bind to the intracellular GPCR–transducer interface change G protein coupling by subtype-specific and predictable mechanisms, enabling structure-guided drug design. We find that the intracellular, core-binding compound SBI-553 switches the G protein preference of NTSR1 through direct intermolecular interactions[3–5], promoting or preventing association with specific G protein subtypes. Modifications to the SBI-553 scaffold produce allosteric modulators with distinct G protein selectivity profiles. Selectivity profiles are probe independent, conserved across species and translate to differences in activity in vivo. Our studies show that G protein selectivity can be tailored with small changes to a single chemical scaffold targeting the receptor–transducer interface. Moreover, given that this pocket is broadly conserved, our findings could provide a strategy for pathway-selective drug discovery that is applicable to the diverse GPCR superfamily.

GPCRs are the largest family of drug targets, accounting for more than one-third of all medicines[6]. Their multiple G protein and β-arrestin signalling partners (transducers) can mediate distinct effects, some beneficial and others deleterious. At the same receptor, different ligands can induce distinct transducer coupling and physiological effects, a phenomenon known as functional selectivity or biased signalling[1].

Compounds that shunt receptor signalling away from one G protein subtype and towards another could be transformative, potentially enabling the separation of on-target therapeutic effects from side effects and the redirection of signalling by receptors responsible for disease[2]. Biased signalling was discovered more than 30 years ago, however, and the promise of compounds with improved therapeutic benefits remains largely unfulfilled. In some instances, there is a clear connection between the changes in receptor conformation induced by the binding of a biased ligand and the type of signalling bias observed[7,8]. More often, the molecular basis of biased agonism is unclear[9], precluding structure-based design.

We propose that small molecules that target the intracellular GPCR–transducer interface can change G protein coupling by subtype-specific and predictable mechanisms. In the intracellular pocket, compounds are positioned to interact directly with transducers. Here, they may serve simultaneously as molecular bumpers and molecular glues. Molecular bumpers sterically prevent protein–protein interactions through overlapping van der Waals (VDW) radii or repulsive electrostatic interactions. Molecular glues stabilize protein–protein interactions through attractive intermolecular forces. Given the sequence diversity of the portion of the G protein that interacts with the GPCR core, it should be possible for a core-binding ligand to change receptor G protein affinity in a subtype-specific manner, thereby switching the receptor's preferred G protein, downstream signalling and physiological effect.

As a proof of concept, we examined NTSR1, a potential drug target for schizophrenia, cancer, substance-use disorders and pain[10]. Balanced NTSR1 agonists activate many transducers, and this results in on-target side effects, including hypothermia[11]. We previously discovered[3–5] SBI-553, a biased NTSR1 agonist that binds intracellularly and preferentially activates β-arrestins over NTSR1's preferred G protein G_q. SBI-553 family compounds attenuate addiction-associated behaviours and reduce pain without the side effects of balanced receptor activation[4,12,13]. Here we show that SBI-553, in addition to conferring β-arrestin bias, switches

[1]Department of Pharmacology, University of Minnesota Twin Cities, Minneapolis, MN, USA. [2]Department of Cell Biology, Duke University, Durham, NC, USA. [3]Graduate School of Pharmaceutical Sciences, Tohoku University, Sendai, Japan. [4]Graduate School of Pharmaceutical Sciences, Kyoto University, Kyoto, Japan. [5]Center for Therapeutics Discovery, Sanford Burnham Prebys Medical Discovery Institute, La Jolla, CA, USA. [6]These authors contributed equally: Madelyn N. Moore, Kelsey L. Person. ✉e-mail: lslosky@umn.edu

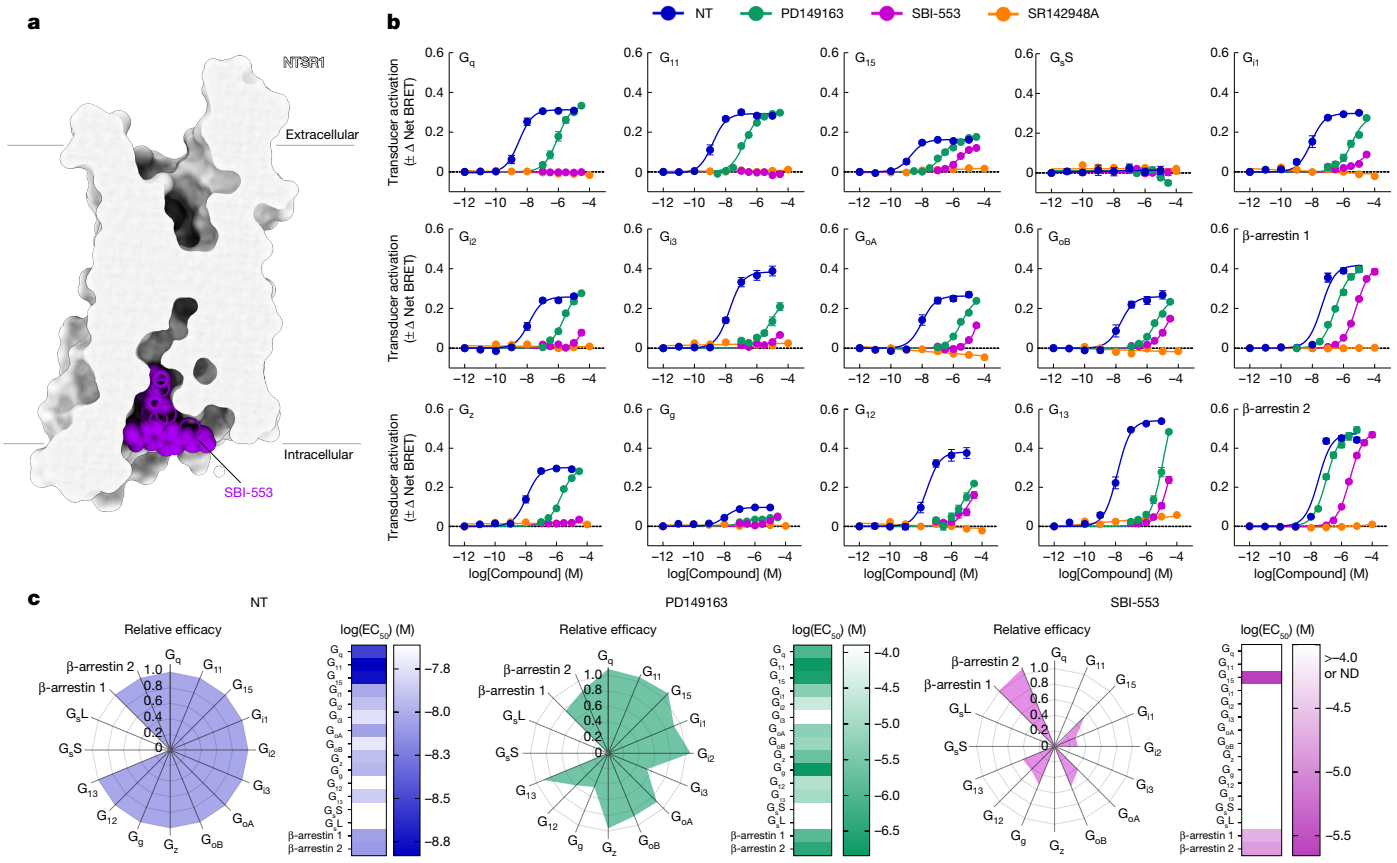

Fig. 1 | The NTSR1 allosteric modulator SBI-553 exhibits transducer-specific efficacy. a, Structure (PDB: 8FN0) showing the position of SBI-553 binding in the NTSR1 core. **b**, Ligand-directed NTSR1 signalling was assessed in HEK293T cells transiently expressing NTSR1 and G protein or β-arrestin activation sensors. G protein activation by TRUPATH and β-arrestin 1 and β-arrestin 2 recruitment by BRET1 was assessed after treatment with the endogenous agonist NT, the NT peptide analogue PD149163, the β-arrestin-biased ligand SBI-553 and the orthosteric antagonist SR142948A. Points were fitted to lines or three-parameter sigmoidal curves, with curve bottom, EC_{50} and top (maximum effect, E_{max}) unconstrained. G_g, gustducin; G_s short, G_sS. **c**, Radar plots depict the extent of transducer activation relative to NT (that is, fold change NT E_{max} for each transducer). Heat maps depict ligand potency. Data are mean ± s.e.m. $n = 4$ independent experiments for G_{oB}, Gg, G_sS and β-arrestins and $n = 3$ independent experiments for all other transducers. G_sL, G_s long; ND, not detected. For curve parameters see Supplementary Table 1. For supporting data, see Extended Data Fig. 1.

NTSR1 G protein subtype preference. We describe the mechanism by which this switch is achieved and use this mechanism to design new compounds with distinct G protein subtype selectivity profiles. Using structural models and high-dimensional structure–activity relationship (SAR) studies, we find that minor modifications to SBI-553 differentially change NTSR1 G protein subtype coupling. Selectivity profiles are conserved across receptor species and translate to differences in efficacy in rodent models. These findings show that G-protein-subtype-selective biased allosteric modulators (BAMs) can be rationally designed, and provide an approach for biased compound discovery that is applicable to the wide array of GPCR therapeutic targets.

Ligand-directed G protein activation by NTSR1

Four families of Gα proteins—$G_{i/o}$, G_q, G_s and $G_{12/13}$—mediate distinct cellular effects[14,15]. Although the specific repertoire varies by tissue, most cells express Gα subunits from multiple families[16–18] and most GPCRs can activate G proteins from more than one family[14,15], enabling diverse signalling. NTSR1 is highly expressed in the gastrointestinal tract and brain, tissues that express nearly all non-visual Gα proteins[16]. We began by characterizing human NTSR1 signalling after stimulation with: (1) the endogenous ligand neurotensin (NT); (2) a mimetic of the NT active fragment PD149163 (ref. 19); (3) the intracellular β-arrestin BAM SBI-553 (refs. 3,4); and (4) the competitive NTSR1 antagonist and inverse agonist SR142948A (refs. 20,21). Using TRUPATH bioluminescence resonance energy transfer (BRET) 2 sensors[22] in HEK293T cells, we assessed ligand-induced activation of 14 Gα proteins (Extended Data Fig. 1a,b). In these assays, NT exhibited extreme promiscuity, activating at least 12 G proteins across 3 families. The only G protein family that NT did not activate in this platform was G_s (Fig. 1b and Extended Data Fig. 1c), as reported previously[22]. NT most potently activated the $G_{q/11}$ family of G proteins.

Compared with NT, PD149163 was a less potent activator and exhibited G-protein-specific potency (Fig. 1b). PD149163 fully agonized all $G_{q/11}$ proteins and some $G_{i/o}$ proteins, but full concentration–response curves (CRCs) were not captured for G_{i3}, G_{12} and G_{13} (Extended Data Fig. 1d). Applied alone, SR142948A had no effect in this assay (Fig. 1b). In line with previous work[4,5], SBI-553 did not activate G_q or G_{11} (Fig. 1b). It did, however, weakly activate other G proteins; namely, G_{15}, G_{i1}, G_{i2}, G_{oA}, G_{oB}, G_g, G_{12} and G_{13} (Fig. 1b and Extended Data Fig. 1d). Saturating responses were not obtained, precluding determination of the half-maximum effective concentration (EC_{50}), but detected activation was mediated by NTSR1 (Extended Data Fig. 1e).

We next used a BRET1-based assay to characterize ligand-induced recruitment of human β-arrestins 1 and 2 to NTSR1 (ref. 4 and Extended Data Fig. 1f). NT, PD149163 and SBI-553 recruited β-arrestins 1 and 2 to NTSR1, whereas SR142948A did not (Fig. 1b). G protein and β-arrestin agonism data were standardized to maximum NT levels and summarized in radar plots (Fig. 1c). These plots highlight that SBI-553 is a low-potency agonist of a subset of G proteins, but not NTSR1's cognate $G_{q/11}$.

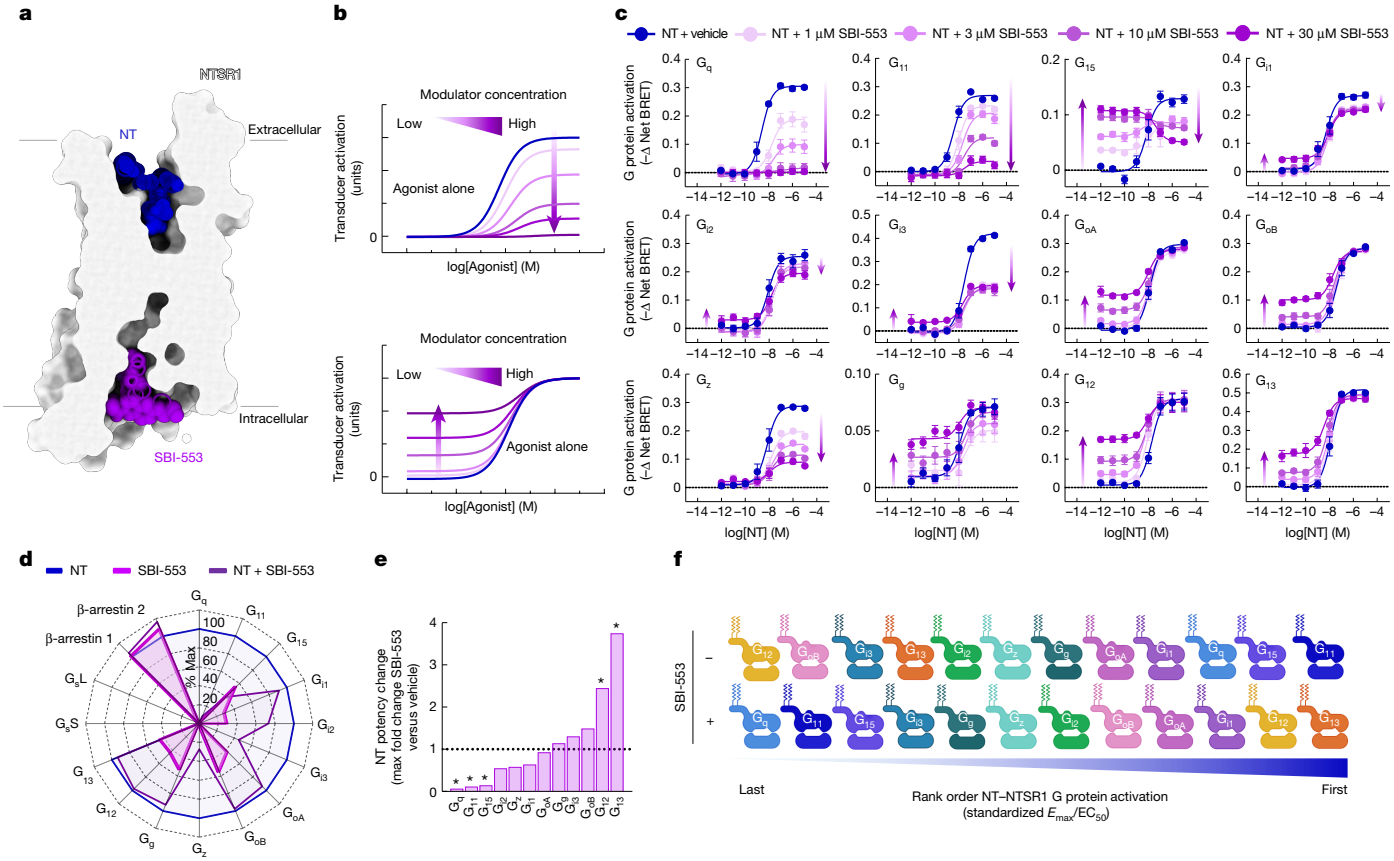

Fig. 2 | SBI-553 biases NT–NTSR1 signalling away from $G_{q/11}$ and towards alternative G protein activation. a, Structure (PDB: 8FN0) showing NTSR1 co-occupied by the active fragment of the NT peptide in the orthosteric pocket and SBI-553 in the receptor core. **b**, Examples of characteristic agonist CRC shifts in the presence of a non-competitive antagonist (top) or an allosteric agonist (bottom). **c**, NT-induced G protein activation was assessed by TRUPATH in the absence and presence of SBI-553 in HEK293T cells transiently expressing NTSR1. **d**, Radar plots depict the extent of activation of each transducer in the presence of NT alone, SBI-553 alone and both NT and SBI-553. The % Max values are standardized to NT E_{max} for each transducer. **e**, Change in apparent NT potency in the presence of SBI-553. NT CRC EC_{50} values were determined for each G protein at the maximum SBI-553 concentration for which a sigmoidal curve could be fit. Data are represented as fold change from vehicle. Asterisks indicate G proteins for which the NT + vehicle curve EC_{50} versus NT + SBI-553 curve EC_{50} have non-overlapping 95% confidence intervals. **f**, Rank order of NT–NTSR1 G protein preference in the absence and presence of 30 μM SBI-553, on the basis of standardized log(E_{max}/EC_{50}). Illustration in **f** created using BioRender (Slosky, L. (2025) https://BioRender.com/jt8g27q). Data are mean ± s.e.m. $n = 3$ independent experiments. For curve parameters, including confidence intervals, see Supplementary Table 2. For supporting data, see Extended Data Figs. 2–4 and Supplementary Fig. 2.

To confirm that SBI-553 exhibits G-protein-subtype-specific effects, we used a transforming growth factor-α (TGFα) shedding assay to assess G protein activation[23] (Extended Data Fig. 1g). In this assay, all G protein sensors are based on the same G_q backbone and G protein subtype specificity is conferred by substitution of the six C-terminal amino acids. Here, NT stimulated NTSR1 to activate all 11 of the G protein sensors, but not a control G protein construct lacking the C terminus (GΔC) (Extended Data Fig. 1h). SBI-553 was a low-potency but full agonist of $G_{12/13}$ and a weak agonist of some $G_{i/o}$ family members (Extended Data Fig. 1h,i). These findings corroborate and extend the previous results, showing that SBI-553 has previously unappreciated G protein agonist activity and that the six C-terminal amino acids of each Gα protein are sufficient to bestow this activity.

Uniform antagonism of NT-induced NTSR1 activation

Because SBI-553 and NT can bind to NTSR1 simultaneously, we next focused on the modulation of NT-induced NTSR1 transducer activation. To verify our ability to generate and identify CRCs that are characteristic of competitive antagonism (Extended Data Fig. 2a,b), we assessed the effect of pretreatment with SR142948A on NT-induced transducer activation. SR142958A pretreatment produced a uniform, concentration-dependent blockade of NT-induced β-arrestin recruitment and G protein activation, regardless of the Gα subtype (Extended Data Fig. 2c,d). In line with a competitive mechanism, SR142948A increased NT's observed EC_{50} in a concentration-dependent manner for all transducers, producing comparable equilibrium dissociation constants (K_B) (Extended Data Fig. 2e). These data showcase the effects of a competitive antagonist that indiscriminately blocks NT-induced transducer activation.

Biasing of NT-induced NTSR1 signalling by SBI-553

In contrast to the action of SR142948A, SBI-553 exhibited transducer-specific allosteric effects. From its intracellular location (Fig. 2a) SBI-553 produced two different activities depending on the transducer evaluated: (1) non-competitive antagonism, as evidenced by a reduction in the height of the NT CRC; and (2) agonism, as evidenced by a rising NT CRC baseline (Fig. 2b). SBI-553 stimulated β-arrestin recruitment to NTSR1 alone and permitted NT-induced β-arrestin recruitment (Extended Data Fig. 2c). In combination with NT, SBI-553 fully antagonized some G proteins (G_q and G_{11}), partially antagonized others (G_{i1}, G_{i2}, G_{i3} and G_z) and was permissive of NT-induced activation of others (G_{oA}, G_{oB}, G_{12} and G_{13}) (Fig. 2c). Unlike a competitive antagonist, SBI-553

did not exert consistent effects on NT EC_{50} values across transducers. SBI-553 increased NT potency at G_{12} and G_{13}, decreased NT potency at G_q, G_{11} and G_{15} and did not change NT potency at other G proteins (Fig. 2e). Notably, the G proteins for which SBI-553 continued to permit NT-induced signalling were the same as those that SBI-553 alone activated (Fig. 2d). The directionality and extent of SBI-553's effect on NT signalling were largely stable with changes in temperature (Extended Data Fig. 3), and consistent over time (Extended Data Fig. 4). The allosteric effects of SBI-553 on NT-induced transducer activation can be described using the operational model with transducer-specific allosteric parameters[2] (Supplementary Fig. 2).

The G-protein-specific effects of SBI-553 were consistent across assays. In the TGFα shedding assay, SBI-553 fully antagonized G_q, partially antagonized G_{i1} and G_{i2} and was permissive of NT-induced G_o and G_{12} activation (Extended Data Fig. 2g). Together, these data suggest that SBI-553 antagonizes NT-induced activation of some G proteins but not others. By doing so, SBI-553 biases NTSR1 not only towards β-arrestin, but also towards a subset of G proteins (Extended Data Fig. 2h), changing NTSR1's most preferred G proteins from those of the $G_{q/11}$ family to those of the $G_{12/13}$ family (Fig. 2f).

SBI-553 acts via a β-arrestin-independent mechanism

The ability of SBI-553 to antagonize NT-mediated G protein activation might arise either from a reduction in the formation of NTSR1–G protein complexes or through the stabilization of signalling-incompetent NTSR1–G protein complexes, as proposed previously[5,24]. To distinguish between these possibilities, we turned to a BRET-based assay of mini-G protein recruitment. Mini-G proteins are modified G proteins that form stable GPCR complexes, permitting the monitoring of complex association[25]. NT stimulation resulted in the recruitment of representative G protein family members mini-G_q, -G_{i1}, -G_s, -G_o and -G_{12} to NTSR1 (Extended Data Fig. 5a–d). In line with SBI-553 inhibiting NTSR1–G_q coupling, SBI-553 fully antagonized NT-induced mini-G_q recruitment (Fig. 3a). SBI-553 partially antagonized the recruitment of mini-G_{i1} and G_s, had little effect on the recruitment of G_o and increased NTSR1–G_{12} association. These data suggest that SBI-553 antagonizes NTSR1 G_q activation by selectively preventing NTSR1–G_q coupling.

β-Arrestins desensitize GPCRs, in part, by occupying the receptor core and occluding G protein binding[26]. SBI-553 might prevent NTSR1–G_q coupling either because SBI-553 binding is incompatible with G_q binding or because SBI-553 stimulates the recruitment of β-arrestin to NTSR1, and β-arrestin, in turn, prevents G_q binding. To address this question, we evaluated the ability of SBI-553 to antagonize NT-induced NTSR1–G_q complex formation in cells lacking β-arrestins 1 and 2 (hereafter referred to as β-arrestin 1/2-null cells)[27]. SBI-553 fully blocked NTSR1–G_q recruitment in β-arrestin 1/2-null cells (Fig. 3b), showing that β-arrestins are not necessary for SBI-553's blockade of NTSR1–G_q coupling. Likewise, agonism of G_{oA} remained intact after ablation of β-arrestins 1 and 2 (Extended Data Fig. 5e–g).

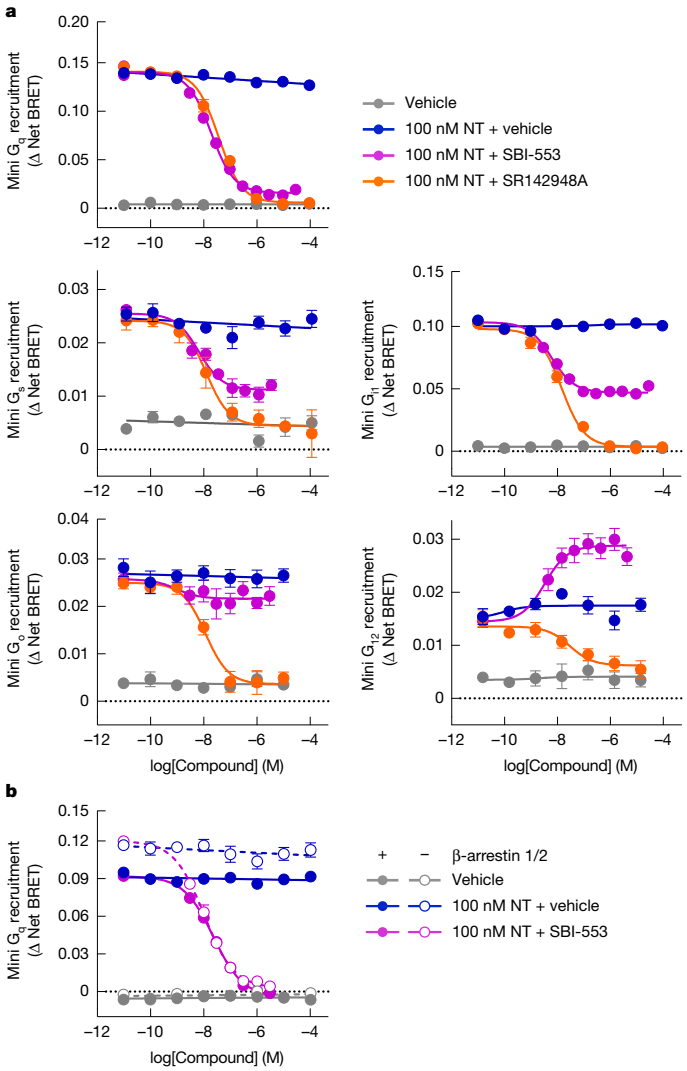

Fig. 3 | SBI-553 blocks NTSR1 coupling with a subset of G proteins through a β-arrestin-independent mechanism. a, NT (100 nM)-induced recruitment of mini-G_q, mini-G_{i1}, mini-G_s, mini-G_o or mini-G_{12} to NTSR1 in HEK293T cells was assessed in the presence of vehicle (blue), SBI-553 (magenta) or SR142948A (orange). Controls received vehicle alone (grey). **b**, NT-induced recruitment of mini-G_q in the absence and presence of SBI-553 was assessed in β-arrestin 1/2-null HEK293 cells (open circles) and their parental control line (solid circles). Cells were pretreated with either SBI-553 or its vehicle before application of 100 nM NT or its vehicle. Data are mean ± s.e.m. $n = 3$ independent experiments. For curve parameters, see Supplementary Table 3. For supporting data, see Extended Data Fig. 5.

Molecular basis of SBI-553's G protein selectivity

Rather than being a consequence of β-arrestin recruitment, SBI-553's antagonism of NTSR1–$G_{q/11}$ activation might result from direct or allosteric occlusion of the binding determinants of $G_{q/11}$. Gα subunits associate with GPCR intracellular cores through their highly variable C termini. To test whether SBI-553 antagonism depended on the primary structure of the G protein C terminus, we created chimeric G proteins in which we swapped the five C-terminal residues between G_{oA} and G_q (Extended Data Fig. 6a). Although SBI-553 was fully permissive of NT-induced G_{oA} activation, SBI-553 antagonized the G_{oA}–G_q chimera, which contained the G_q C terminus (G_{oA}(G_q C-term); Fig. 4a). Conversely, SBI-553 acted as a partial rather than a full antagonist of the G_q–G_{oA} chimera (G_q(G_{oA} C-term); Extended Data Fig. 6b). We created a larger C-terminal swap, removing the 13 C-terminal residues from G_q and replacing them with those from G_{oA}. This G_q(Δ247–259G_{oA}) was insensitive to antagonism by SBI-553 at all concentrations except the highest (Fig. 4b). Together, these data suggest that SBI-553's G protein subtype selectivity is a result of the different primary structures of the Gα C termini.

To determine the residues responsible for this change in sensitivity, we aligned Gα C termini, identifying four residues unique to $G_{q/11}$ (Fig. 4c). To evaluate the individual contributions of these residues to SBI-553's G_q antagonism, we replaced each G_q residue with its corresponding G_{oA} residue in the TRUPATH construct: V359Y (helix position H5.26), N357G (H5.24), Y356C (H5.23) and L351N (H5.18). NT continued to activate these mutants (Extended Data Fig. 6c–e) and SBI-553 remained a full antagonist of all constructs (Fig. 4d). Crucially, no point mutant reproduced the reversal in sensitivity to SBI-553 antagonism seen with the full C-terminal swap.

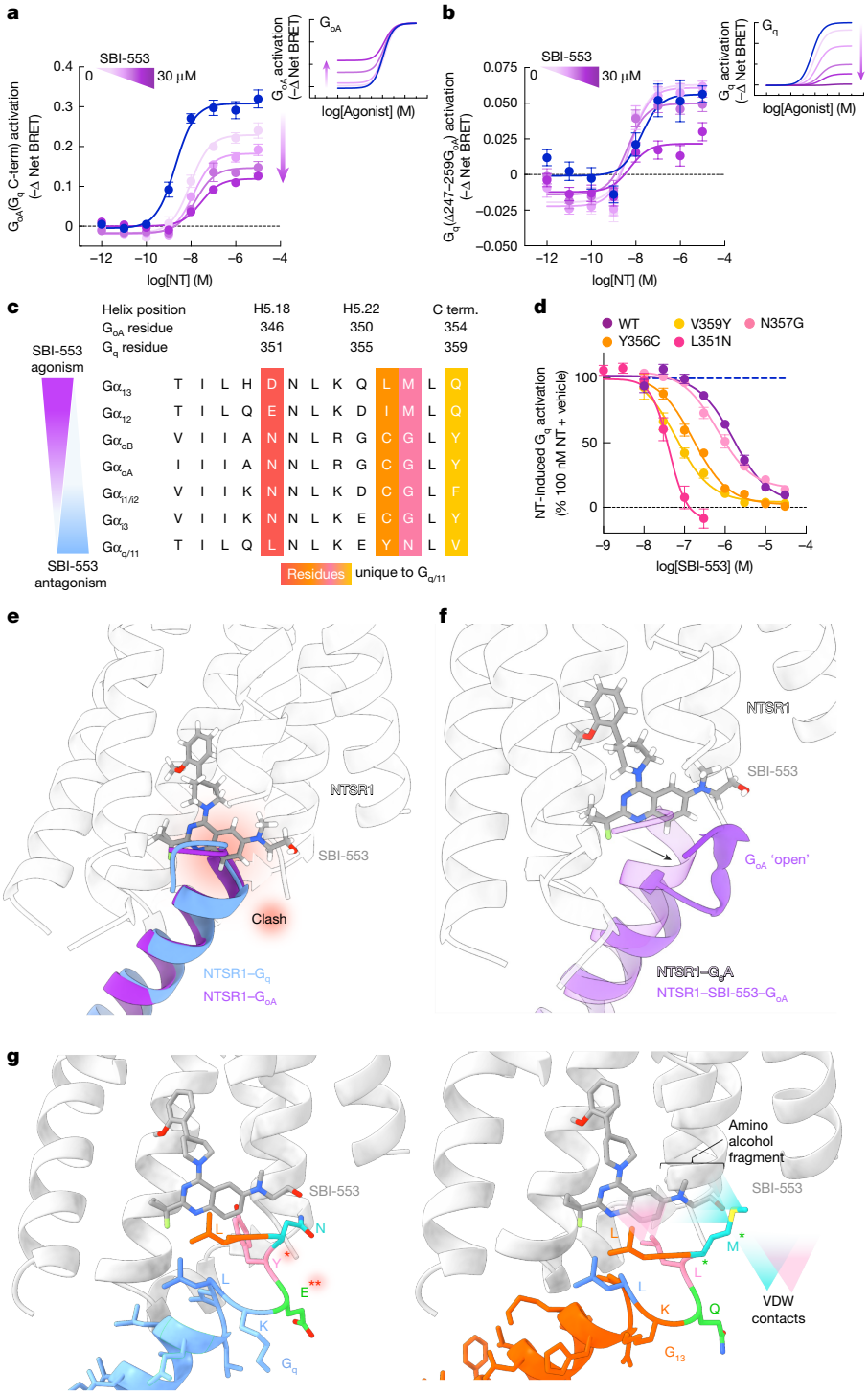

Fig. 4 | The sensitivity of a Gα protein to SBI-553 antagonism is determined by the ability of its C terminus to adopt an alternative shallow-binding conformation. a,**b**, The sensitivity of G proteins to SBI-553 antagonism can be reversed by exchanging their C termini. **a**, Swapping $G_o^{A\nu}$'s five C-terminal amino acids for those of G_q confers sensitivity to SBI-553 antagonism. Inset, effect of SBI-553 on NT-induced activation of WT G_{oA}, for reference. $n = 3$ independent experiments. **b**, Swapping G_q's 13 C-terminal amino acids for those of G_{oA} reduces the antagonist potency and efficacy of SBI-553. Inset, effect of SBI-553 on NT-induced activation of WT G_q, for reference. $n = 5$ independent experiments. **c**, Alignment of G protein C termini. **d**, Single-amino-acid substitutions on G_q's C terminus are insufficient to render G_q permissive of SBI-553. Effect of G_q mutagenesis on the ability of SBI-553 to antagonize G_q activation by 100 nM NT in the TRUPATH assay. $n = 3$ (WT, V369Y), 4 (Y356C, N357G) or 7 (L351N) independent experiments. **e**,**f**, SBI-553-induced shallow-binding 'open' G_{oA} conformation. **e**, Docking of SBI-553 in the PDB: 8FN1 and PDB: 8FMZ structures suggests that both G_{oA} and G_q should clash with SBI-553. **f**, Superposition of the PDB: 8FN1 and PDB: 8FN0 structures illustrates that, in the presence of SBI-553, G_{oA} adopts an alternative 'open' conformation to accommodate SBI-553 binding. **g**, Homology modelling indicates that some NTSR1–SBI-553 'open'-position G protein complexes are more energetically favourable than others. In silico homology models were created based on the 'open' NTSR1–SBI-553-bound G_{oA} conformation by changing the 13 C-terminal amino acids. Single red asterisk indicates loss of contact with NTSR1 TM3 and TM4, as compared with the G_q 'closed' conformation; double red asterisk indicates the need to adopt an energetically unfavourable positive phi angle; single green asterisk indicates the formation of complex-stabilizing VDW contacts with SBI-553. All graphical data are mean ± s.e.m. For curve parameters, see Supplementary Table 4. For supporting data, see Extended Data Fig. 6 and Supplementary Figs. 3–5.

To understand why changes at single positions were insufficient to reduce the sensitivity of G_q to SBI-553 antagonism, we turned to structural data. SBI-553 binds to NTSR1 at an intracellular site in the hydrophobic region of NTSR1's core, where it is positioned to interact with associating transducers[5,28]. We previously generated structures of NTSR1–NT in complex with mini-Go_A in the absence (Protein Data Bank (PDB) ID: 8FN1) and presence (PDB: 8FN0) of SBI-553, as well as NTSR1–NT in complex with mini-G_q in the absence of SBI-553 (PDB: 8FMZ; Extended Data Fig. 6f). In the absence of SBI-553, the NTSR1-bound G_{oA} and G_q C termini exist in a 'closed' α-helical state. Superposition of these structures reveals a nearly complete overlap of the G_{oA} and G_q C termini in the receptor core. Docking SBI-553 at its observed binding site in these structures results in steric clashes with both G_{oA} and G_q (Fig. 4e). From PDB 8FN0 (ref. 5), we see that, in the presence of SBI-553, the G_{oA} C terminus adopts an alternative, shallow-binding 'open' conformation. The G_o helix tilts 14° toward transmembrane helix (TM) 1 and slightly unwinds over the last five residues, protruding 4 Å less deeply into the receptor core (Fig. 4f). In this 'open' orientation, G_{oA} makes VDW contact with the hydroxyl side chain, quinazoline C8 and fluorine of SBI-553.

Superimposing GPCR–G protein complexes from the PDB failed to identify an analogous orientation, suggesting that the Go_A 'open' conformation is unique (Supplementary Fig. 3). On the basis of this structure[5], SBI-553 mediates G protein activation by inducing active conformations of both the NTSR1 core and the Gα protein. SBI-553 forms an electrostatic interaction with the arginine (R) of NTSR1's E/DRY motif, disrupting the ability of this highly conserved motif to stabilize the receptor inactive conformation. In addition, SBI-553 positions the G_{oA} C-terminal helix in an unwound, rotated conformation reminiscent of G protein activation state intermediates[29] (Supplementary Fig. 4).

Efforts to resolve a NTSR1–SBI-553-G_q structure have been unsuccessful, yielding NTSR1–G_q complexes that lack SBI-553 density[5], probably owing to incompatibility between SBI-553 binding and G_q coupling. To predict SBI-553 activity for a range of G proteins, we built in silico homology models for G_q, G_{i1}, G_{oB}, G_i, G_{i2}, G_{i3}, G_{12} and G_{13}. In an optimized NT–NTSR1–SBI-553–G_{oA} 'open' position structure, we replaced the 13 C-terminal residues of G_{oA} with those of the other G proteins (Fig. 4g and Supplementary Fig. 5). These models reveal multiple structural differences that might increase the energy of this 'open' conformation for $G_{q/11}$ relative to G_{oA} and provide a rational explanation for SBI-553's G-protein-specific effects. For example, forcing the glutamic acid residue of $G_{q/11}$ at H5.22 to adopt a positive phi angle, although allowed, is energetically unfavourable. For both G_{12} and G_{13}, methionine at H5.24 must adopt a slightly higher energy conformation with gauche interactions, but this small penalty is compensated by close contact with the SBI-553 amino alcohol fragment. In addition to those contacts identified for G_{oA}, the isoleucine residue of G_{12} and the leucine residue of G_{13} at H5.23 make productive VDW contact with SBI-553, further increasing complex stability. These models suggest that SBI-553 promotes association with Gα proteins that can adopt an alternative shallow-binding conformation, and prevents association with subtypes for which this conformation is energetically unfavourable.

BAMs with distinct G protein selectivity profiles

On the basis of these models, we undertook SAR studies to determine whether SBI-553's G protein selectivity profile could be changed by modifying its structure. We hypothesized that SBI-553 analogues would displace or stabilize G protein interactions depending on the position, size and direction of substitution. We focused on the fluorine geminal to SBI-553's cyclopropyl ring and quinazoline C6, C7 and C8 because, according to the model, these regions interact with G protein C termini.

We created a panel of 29 analogues of SBI-553 and assessed them for their ability to antagonize NT-induced G_q, G_i, G_o and G_{12} activation and to agonize β-arrestin (Extended Data Figs. 7 and 8). A summary of the SAR is shown in Fig. 5a and Supplementary Fig. 6. We identified compounds with two-to-threefold-increased β-arrestin potency and comparable G_q inhibition potency relative to SBI-553, suggesting that these properties can vary independently (Supplementary Fig. 7). Although most compounds retained β-arrestin agonism, some exhibited neither G protein antagonism nor β-arrestin agonism, probably owing to loss of NTSR1 affinity (Supplementary Fig. 8). Notably, small changes to the SBI-553 scaffold induced pronounced differences in G protein selectivity.

Modelling predicted that C7 quinazoline substitution would disrupt G_{oA} signalling. SBI-0647342 (SBI-342), a dimethoxy-quinazoline analogue of SBI-553 (Fig. 5b), exhibited reduced NT-induced G_{oA} activation (Extended Data Fig. 9a). Its G_q antagonism was modestly reduced relative to SBI-553, but its β-arrestin agonism was preserved (Extended Data Fig. 9a). The effect of SBI-342 on NT's full CRC curve confirmed that it lacked G_{oA} agonism and reduced maximal NT G_{oA} activation by around 60% compared with SBI-553 (Extended Data Fig. 9b). The action of SBI-342 was specific to NT–NTSR1, because it did not directly change G_{oA} activation in cells without NTSR1 (Extended Data Fig. 9c) and did not impair the ability of other GPCRs to activate G_o (Extended Data Fig. 9d). In both the TGFα shedding and G_o recruitment assays, SBI-342 fully blocked NT-induced G_o activation (Extended Data Fig. 9e,f).

SAR studies indicate that the change in G_{oA} permissiveness is attributable to SBI-342's 7-methoxy group rather than to the methyl substitution on the cyclopropyl group (Extended Data Fig. 9g). A comparison of SBI-553 versus SBI-342 in the SBI-553-binding pocket of the NTSR1–SBI-553–G_{oA} structure reveals a clash between the C7 methoxy of SBI-342 and a backbone carbonyl of G_{oA}, which is absent with SBI-553 (Fig. 5d and Supplementary Fig. 9). This example highlights the predictive and explanatory value of structure-based BAM design.

Other SBI-553 analogues produced unexpected results. For example, compound SBI-0646593 (SBI-593) an analogue with C6 methoxy and C7 trifluoromethyl substitution (Fig. 5b), was more permissive of NT-induced G_q activation than was SBI-533 (Extended Data Fig. 9a). Its effects on other G proteins did not differ, and it retained β-arrestin agonism (Extended Data Fig. 9a). Comparing the effects of SBI-553 and SBI-593 on NT's full CRC curve confirmed that SBI-593 reduced NT G_q activation by only 30% (Extended Data Fig. 9h), an action that was specific to NT–NTSR1 (Extended Data Fig. 9i) and consistent across assays (Extended Data Fig. 9j,k).

SAR and modelling data suggest that the change in G_q permissiveness with SBI-593 is attributable to its trifluoromethyl quinazoline substituent (Extended Data Fig. 9g). Docking SBI-593 in the SBI-553-binding pocket of the NTSR1–G_q structure indicates that it should sterically exclude G_q (Supplementary Fig. 10a). The preservation of G_q activity with SBI-593 requires that the G_q C terminus adopt an alternate binding pose. In molecular dynamics simulations of the NTSR1–G_q–NT–SBI-593 complex, G_q's C-terminal helix unwinds and tilts toward NTSR1's TM4 and intracellular loop 1 to avoid clashing with SBI-593 (Fig. 5e and Supplementary Fig. 10). This alternative, shallow-binding conformation is distinct from the G_{oA} 'open' orientation and is stabilized by multiple polar and non-polar interactions with NTSR1 (Extended Data Fig. 9l). VDW interactions between the trifluoromethyl of SBI-593 and G_q, which are absent for SBI-553 (Fig. 5f), probably explain why G_q does not adopt this posture in the presence of SBI-553.

We generated allosteric CRC families for NT with SBI-342, SBI-593 and SBI-553 for G_q, G_{i1}, G_{oA}, G_{12} and β-arrestin 2 (Extended Data Fig. 9m), and used these curves to calculate modulator-specific cooperativity and intrinsic efficacy values (Supplementary Fig. 11). Maximal NT-induced G protein activation in the presence of each of these BAMs is summarized in radar plots. As is evident from these plots, SBI-553, SBI-342 and SBI-593 exert differential effects on NT-induced transducer activation (Fig. 5b). Notably, neither SBI-342 nor SBI-593 activate G_{oA} or $G_{12/13}$ alone. Like SBI-553 (refs. 3,30), however, SBI-342 and SBI-593 are selective for NTSR1 (Extended Data Fig. 10a–c). These studies show

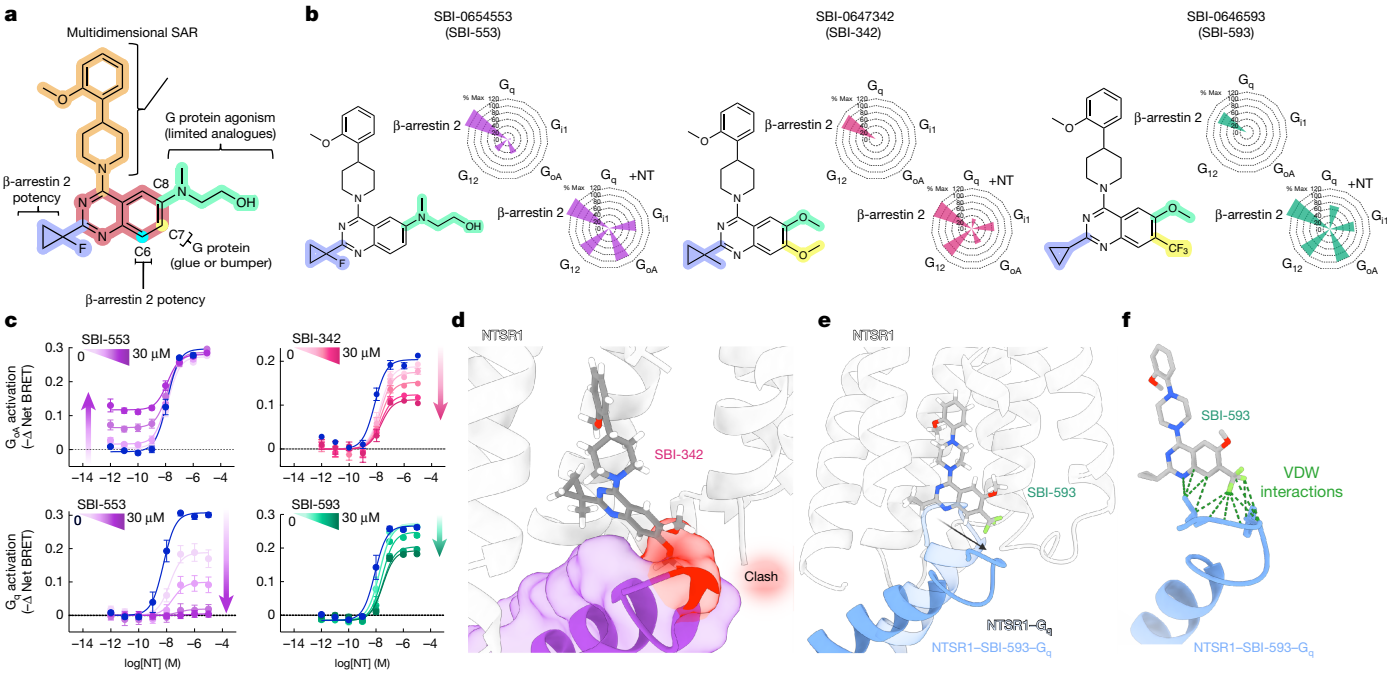

Fig. 5 | Discovery of SBI-553 analogues with distinct G protein selectivity profiles. a, Multidimensional SAR of SBI-553. **b**, Structures of SBI-553 and analogues SBI-342 and SBI-593 with radar plots summarizing the extent of transducer activation induced by SBI-553, SBI-342 and SBI-593 alone (compounds up to 30 μM, top) and in the presence of NT (compounds up to 30 μM, bottom). Values reflect % NT E_{max} at the highest compound concentration relative to NT in the presence of vehicle. In HEK293T cells transiently expressing NTSR1, G protein activation was assessed by TRUPATH, and β-arrestin recruitment was assessed by BRET. For underlying data, see Extended Data Fig. 9m. Data are mean of $n = 3$ independent experiments per compound per transducer. **c**, Top, NT-induced activation of G_{oA} in the presence of SBI-553 or SBI-342. Bottom, NT-induced activation of G_q in the presence of SBI-553 or SBI-593. SBI-553 plots were originally presented in Fig. 2c and are shown here to facilitate analogue comparison. Data are mean ± s.e.m. $n = 3$ independent experiments. **d**, SBI-553 can co-occupy NTSR1 with G_{oA}'s C terminus in its 'open' position, whereas the 9-methoxy group of SBI-342 clashes with G_{oA}. **e**, Molecular dynamics simulations indicate a repositioning of the G_q C terminus within the NTSR1 core. $n = 3$ for 100 nanoseconds (ns) and $n = 3$ for 300 ns. Representative image from a minimized low-energy frame. **f**, Attractive VDW contacts between SBI-593 and the G_q C terminus in its new position are shown as dotted green lines. For curve parameters, see Supplementary Table 5. For supporting data, see Extended Data Figs. 7–10 and Supplementary Figs. 6–11.

that the G protein selectivity of an allosteric modulator can be modified by minor modifications to a single scaffold.

G protein selectivity affects BAM activity in vivo

To determine whether BAMs with different G protein selectivity profiles differ in their in vivo activities, we turned to a model of NTSR1-agonist-induced hypothermia. NT and PD149163 activation of central NTSR1 receptors reduces core body temperature in rats and mice[4,11,31]. SBI-553 can fully block PD149163-induced hypothermia[4]. Because NT mobilizes intracellular calcium in neurons that regulate body temperature[11], $G_{q/11}$ activation leads to calcium mobilization, and $G_{q/11}$ proteins are the only ones that SBI-553 fully antagonizes (Fig. 2). NTSR1–$G_{q/11}$ activation is likely to mediate PD149163-induced hypothermia. As such, we hypothesized that SBI-593, which only partially blocks NTSR1–G_q activation, would be less effective than SBI-553 in countering PD139163-induced hypothermia in mice. To test this, we first verified that PD149163-induced hypothermia in mice is mediated by NTSR1. Indeed, PD149163 produced a dose-dependent reduction in core body temperature in wild-type (WT) mice, but not in *Ntsr1*-knockout (KO; *Ntsr1*$^{-/-}$) mice (Fig. 6a and Extended Data Fig. 12a).

We next asked whether SBI-553 and SBI-593 function similarly across receptor species[32]. The SBI-553-binding pocket of NTSR1 is highly conserved across mammals, and the signalling signatures of SBI-553 and SBI-593 were likewise conserved across mouse, rat, and human NTSR1 (Fig. 6b and Extended Data Fig. 11a–c). Finally, we assessed probe dependence, a phenomenon in which an allosteric modulator exerts distinct effects on receptor signalling depending on the specific orthosteric ligand that is bound to the receptor[33]. The signalling profiles of SBI-553 and SBI-593 were unaffected by a change in orthosteric agonist from NT to PD149163, exhibiting probe independence (Fig. 6b and Extended Data Fig. 11c–e).

To assess the ability of SBI-553 and SBI-593 to attenuate PD149163-induced hypothermia after systemic administration, mice received SBI-553 (12 mg kg^{-1}, intraperitoneally (i.p.)), SBI-593 (12 mg kg^{-1}, i.p.) or their respective vehicles before treatment with PD149163 (0.15 mg kg^{-1}, i.p.) (Extended Data Fig. 12b). SBI-553 attenuated PD149163-induced hypothermia, whereas SBI-593 did not (Fig. 6c). Because PD149163-induced hypothermia is centrally mediated, we evaluated the effects of these compounds after local delivery to the brain. NT produces hypothermia after microinjection into several brain regions[34], including the nucleus accumbens (NAc) in mice[35]. In mice with bilateral cannulas targeting the NAc core (Extended Data Fig. 12c–e), microinjection of PD149163 reduced core body temperature through an NTSR1-dependent mechanism (Extended Data Fig. 12f). To determine the effect of SBI-553 and SBI-593 on this response, mice received SBI-553 (10 μg, bilateral, intra-NAc), SBI-593 (10 μg, bilateral, intra-NAc) or vehicle before intra-NAc treatment with PD149163 (Fig. 6d and Extended Data Fig. 12g). SBI-553 reduced PD149163-induced hypothermia, whereas SBI-593 did not (Fig. 6e and Extended Data Fig. 12h). When all doses were increased tenfold, both compounds reduced PD149163-induced hypothermia, but the proportion of mice exhibiting a complete inhibition differed, with 67% of the SBI-553-treated mice exhibiting complete inhibition, compared with 0% of the SBI-593-treated mice (Extended Data Fig. 12i–m). Reductions in agonist-induced hypothermia are likely to be attributable to G_q antagonism and not β-arrestin agonism, because genetic ablation

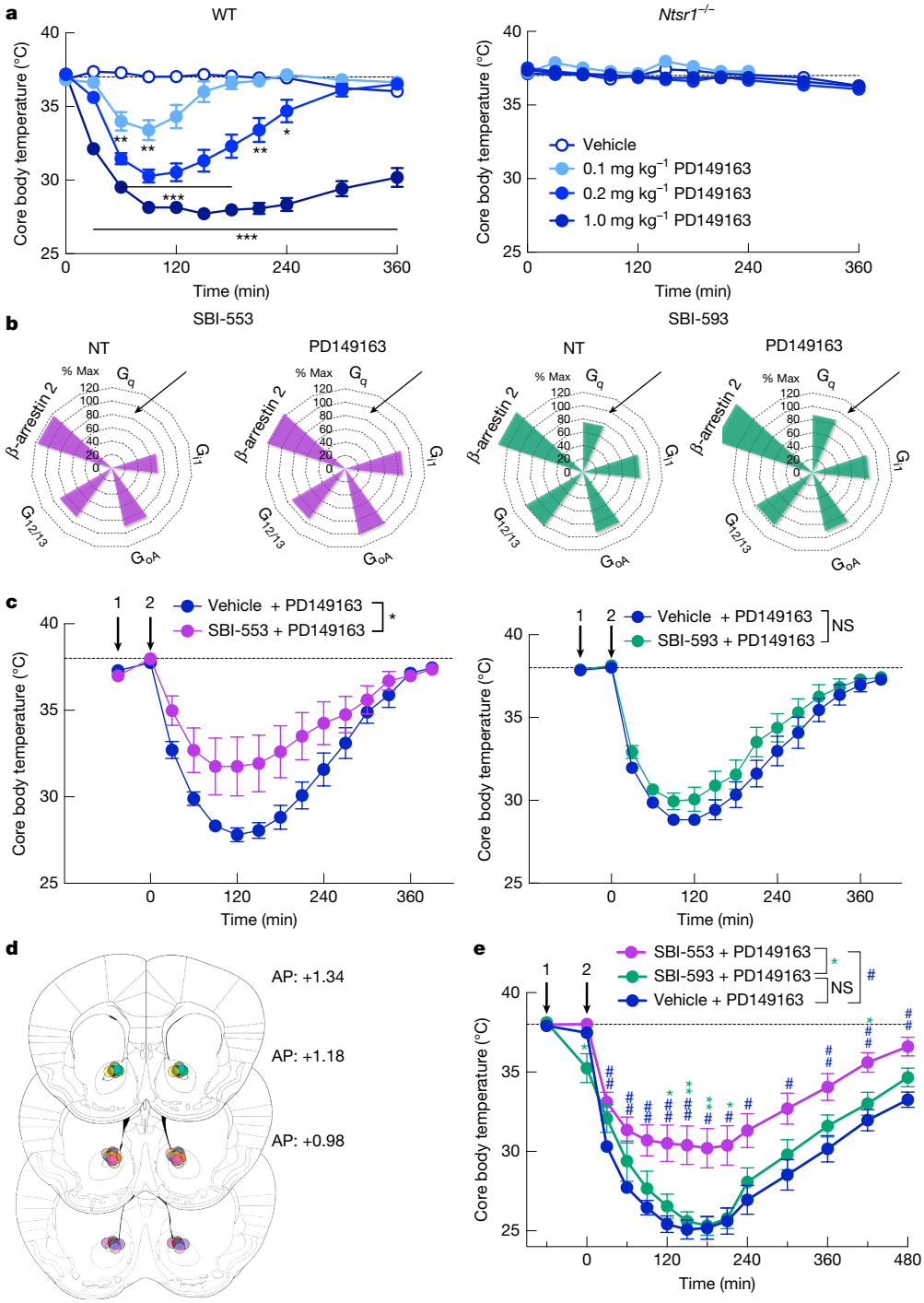

Fig. 6 | SBI-593 does not effectively block NTSR1-agonist-induced, G_q-mediated hypothermia in mice. a, Systemic PD149163 administration induces NTSR1-dependent hypothermia in mice. Effect of PD149163 (0.1–1.0 mg kg^{-1}, i.p.) on core body temperature in WT and *Ntsr1*$^{-/-}$ mice. *n* (mice per group) = 9 WT, 8 *Ntsr1*$^{-/-}$ vehicle; 10 WT, 6 *Ntsr1*$^{-/-}$ 0.1 mg kg^{-1}; 17 WT, 8 *Ntsr1*$^{-/-}$ 0.2 mg kg^{-1}; 14 WT, 8 *Ntsr1*$^{-/-}$ 1.0 mg kg^{-1}. Data analysed by two-way repeated measures ANOVA followed by Dunnett's multiple comparisons test. WT $F_{Treatment}(3,46) = 67.62$, $P < 0.0001$. $^{*}P < 0.05$, $^{**}P < 0.01$, $^{***}P < 0.001$. **b**, SBI-593 incompletely antagonizes PD149163-induced G_q activation by NTSR1. Effects of SBI-553 and SBI-593 on PD149163-induced transducer activation at mouse NTSR1. Arrows highlight consistency in SBI-553's full and SBI-593's incomplete G_q antagonism across receptor species and orthosteric agonists. Data are mean from *n* = 3 independent experiments per receptor species, compound and agonist. Underlying data in Extended Data Fig. 11. **c**, Systemic SBI-593 administration does not attenuate PD149163-induced hypothermia. Effect of SBI-553 (12 mg kg^{-1}, i.p.) or SBI-593 (12 mg kg^{-1}, i.p.) pretreatment versus their respective vehicles on PD149163 (0.15 mg kg^{-1}, i.p.)-induced hypothermia. *n* = 8 per group. Data 30–240 min after treatment were analysed by two-way repeated measures ANOVA. SBI-553 $F_{Treatment}(1,14) = 5.36$, $P = 0.0362$, $^{*}P < 0.05$. SBI-593 $F_{Treatment}(1,14) = 2.61$, $P = 0.1284$ (NS, not significant). **d**, Mice were implanted with intracranial cannulas targeting the NAc core. Images depict cannula placements. Numbers denote mm in front of bregma. AP, anterior–posterior. Brain illustration adapted with permission from ref. 53, Elsevier. **e**, Effect of intra-NAc SBI-553 (10 µg, bilateral), SBI-593 (10 µg, bilateral) or vehicle on PD149163 (0.19 ng, bilateral, intra-NAc)-induced hypothermia. Data were analysed by mixed-model ANOVA followed by Tukey's multiple comparisons test. $F_{Treatment}(2,29) = 7.27$, $P = 0.0028$. $^{*,\#}P < 0.05$; $^{**,\#\#}P < 0.01$. *n* (mice per group) = 12 vehicle, 12 SBI-553 and 8 SBI-593. For additional information on comparisons, see Supplementary Table 6. For supporting data, see Extended Data Fig. 12.

and pharmacological inhibition studies indicate that β-arrestin is not an effective brake on PD149163 hypothermia at the doses evaluated (Extended Data Fig. 12n–u). Together, these findings suggest that SBI-593 is less effective than SBI-553 at blocking NTSR1-agonist-induced, $G_{q/11}$-mediated hypothermia, indicating that BAMs with distinct G protein selectivity profiles can exhibit different in vivo efficacies.

Discussion

Previous studies suggest that promiscuous GPCR–G protein coupling is the norm: 73% of 124 GPCRs evaluated in one assessment[14] and 71% of 100 GPCRs evaluated in another[15] activated multiple G proteins across families. Compounds that shunt signalling towards some G protein pathways and away from others are likely to enable the development of therapeutics that produce desired actions with reduced side effects and the reimagining of established therapeutic targets for new indications. BAMs that bind to the GPCR–transducer interface change G protein selectivity in specific and predictable ways, enabling rational design.

We assessed ligand-directed NTSR1 signalling using a highly comprehensive transducer panel—a strategy made possible by the expanding toolkit for monitoring GPCR–transducer coupling in live cells in real time[15,22,23]. The intracellular NTSR1 BAM SBI-553 has previously unappreciated G protein activity. SBI-553 biased NT–NTSR1 not only away from G_q and towards β-arrestin recruitment, but also towards alternative G protein coupling (that is, G_{oA}, G_{oB}, G_{12} and G_{13}). With this observation, SBI-553 joins a short list of allosteric molecules that have been documented to modulate GPCR G protein subtype selectivity, including a small molecule at the prostaglandin $F_{2\alpha}$ receptor[36], an autoantibody at the calcium-sensing receptor[37] and the gadolinium ion at the metabotropic glutamate receptor 1α (mGluR1α)[38].

Homology modelling indicated that SBI-553 directed NT-induced G protein activation towards G proteins whose C termini could adopt an alternative, shallow-binding conformation, and away from G proteins for which this conformation is energetically disfavoured. To test the hypothesis that changes to the SBI-553 scaffold affect NTSR1 G protein coupling in a subtype-specific manner, we used structural models to design a panel of SBI-553 derivatives, and undertook high-dimensional SAR studies. This effort resulted in molecules that differentially change the NTSR1–G protein signalling landscape. Thus, although the surface area between NTSR1 and a G protein is limited, this site is accessible to small molecules. Furthermore, despite the C termini of G protein subtypes differing by only a handful of residues, small molecules can achieve subtype-specific regulation.

Our screen produced some unexpected results, in part because G protein C termini can adopt multiple conformations. Our predictions are complicated by ligand-specific recruitment of GPCR kinases and conformational changes in NTSR1 and associating transducers. Extensive high-dimensional SAR, structures of NTSR1 bound to G protein subtypes in the presence and absence of BAMs and assessments of NTSR1–G protein dynamics will improve predictive models. Nonetheless, the distinct G-protein-selectivity fingerprints of SBI-553, SBI-342 and SBI-593 are a proof of concept that one can switch the G protein preference of a GPCR with minor chemical modifications to a single scaffold.

SBI-553 and its derivatives show complex allosteric effects. Adding to this complexity is the possibility that these ligands direct signalling differently at distinct locations in the cell. GPCR G protein coupling preference is location dependent[39], and both NT and SBI-553 stimulate NTSR1 trafficking[4]. Another layer of complexity is the presence of 5 β isoforms and 12 γ isoforms of G protein. Assessments of the combinatorial effects of αβγ heterotrimers are needed, because βγ isoforms can exhibit tissue-specific expression, combinatorial restrictions and effector preferences[40].

The only G protein not activated by NTSR1 in the TRUPATH platform was G_s, which was probably a consequence of assay insensitivity[22], because functional coupling of NTSR1 to G proteins of the G_q, $G_{i/o}$ and G_s families has been shown previously[41–45]. In vivo, NTSR1 G protein coupling might be cell- and tissue-type dependent, driven by the relative availability of transducers in the receptor's microdomain[46].

Crucially, the use of intracellular modulators to change G protein selectivity is likely to be transferrable to a wide array of GPCRs. Mounting evidence suggests that many—if not most—GPCRs have an intracellular binding pocket that is accessible to small molecules[47,48]. In a broadly conserved mechanism, agonist binding causes the cytoplasmic end of TM6 to move outwards, opening the intracellular pocket for G protein signalling[49]. The consequence of this movement is the creation of a pocket with high ligandability[50]. Indeed, compounds that bind to the intracellular domain within the 7TM bundle have been described for six other class A receptors (CCR2, CCR9, CCR7, CXCR2, β_2AR, GPR61) and the class B PTH1R receptor[48,51,52]. Although these molecules are at present classified as agonists or antagonists, modifications to the portions that extend into the intracellular cavity could confer transducer selectivity.

Much remains unknown, including the relative expression levels and availability of transducers, how these levels change by cell type and disease state and the consequences of differential coupling to G proteins in the same family. Work is needed to determine—for NTSR1 and for GPCRs broadly—which signalling pathways are desirable and which are undesirable in contexts of health and disease. As this information becomes available, we are now equipped with the tools to develop small-molecule therapeutics with precise pathway selectivity.

Online content

Any methods, additional references, Nature Portfolio reporting summaries, source data, extended data, supplementary information, acknowledgements, peer review information; details of author contributions and competing interests; and statements of data and code availability are available at https://doi.org/10.1038/s41586-025-09643-2.

1. Kolb, P. et al. Community guidelines for GPCR ligand bias: IUPHAR review 32. *Br. J. Pharmacol.* **179**, 3651–3674 (2022).
2. Slosky, L. M., Caron, M. G. & Barak, L. S. Biased allosteric modulators: new frontiers in GPCR drug discovery. *Trends Pharmacol. Sci.* **42**, 283–299 (2021).
3. Pinkerton, A. B. et al. Discovery of β-arrestin biased, orally bioavailable, and CNS penetrant neurotensin receptor 1 (NTR1) allosteric modulators. *J. Med. Chem.* **62**, 8357–8363 (2019).
4. Slosky, L. M. et al. β-Arrestin-biased allosteric modulator of NTSR1 selectively attenuates addictive behaviors. *Cell* **181**, 1364–1379 (2020).
5. Krumm, B. E. et al. Neurotensin receptor allosterism revealed in complex with a biased allosteric modulator. *Biochemistry* **62**, 1233–1248 (2023).
6. Lorente, J. S. et al. GPCR drug discovery: new agents, targets and indications. *Nat. Rev. Drug Discov.* **24**, 458–479 (2025).
7. Wingler, L. M. et al. Angiotensin and biased analogs induce structurally distinct active conformations within a GPCR. *Science* **367**, 888–892 (2020).
8. He, F. et al. Allosteric modulation and G-protein selectivity of the Ca^{2+}-sensing receptor. *Nature* **626**, 1141–1148 (2024).
9. Sachdev, S., Creemer, B. A., Gardella, T. J. & Cheloha, R. W. Highly biased agonism for GPCR ligands via nanobody tethering. *Nat. Commun.* **15**, 4687 (2024).
10. St-Gelais, F., Jomphe, C. & Trudeau, L. E. The role of neurotensin in central nervous system pathophysiology: what is the evidence? *J. Psychiatry Neurosci.* **31**, 229–245 (2006).
11. Tabarean, I. V. Neurotensin induces hypothermia by activating both neuronal neurotensin receptor 1 and astrocytic neurotensin receptor 2 in the median preoptic nucleus. *Neuropharmacology* **171**, 108069 (2020).
12. Guo, R. et al. Arrestin-biased allosteric modulator of neurotensin receptor 1 alleviates acute and chronic pain. *Cell* **188**, 4332–4349 (2025).
13. Gereau, G. B. et al. Biased allosteric modulator of neurotensin receptor 1 reduces ethanol drinking and responses to ethanol administration in rodents. *Addict. Neurosci.* **13**, 100185 (2024).
14. Masuho, I. et al. Rules and mechanisms governing G protein coupling selectivity of GPCRs. *Cell Rep.* **42**, 113173 (2023).
15. Avet, C. et al. Effector membrane translocation biosensors reveal G protein and βarrestin coupling profiles of 100 therapeutically relevant GPCRs. *eLife* **11**, e74101 (2022).
16. Uhlen, M. et al. Tissue-based map of the human proteome. *Science* **347**, 1260419 (2015).
17. Yao, Z. et al. A high-resolution transcriptomic and spatial atlas of cell types in the whole mouse brain. *Nature* **624**, 317–332 (2023).
18. Hauser, A. S. et al. Common coupling map advances GPCR-G protein selectivity. *eLife* **11**, e74107 (2022).

19. Wustrow, D. J. et al. Reduced amide bond neurotensin 8–13 mimetics with potent in vivo activity. *Bioorg. Med. Chem. Lett.* **5**, 997–1002 (1995).
20. Gully, D. et al. Biochemical and pharmacological activities of SR 142948 A, a new potent neurotensin receptor antagonist. *J. Pharmacol. Exp. Ther.* **280**, 802–812 (1997).
21. Deluigi, M. et al. Complexes of the neurotensin receptor 1 with small-molecule ligands reveal structural determinants of full, partial, and inverse agonism. *Sci. Adv.* **7**, eabe5504 (2021).
22. Olsen, R. H. J. et al. TRUPATH, an open-source biosensor platform for interrogating the GPCR transducerome. *Nat. Chem. Biol.* **16**, 841–849 (2020).
23. Inoue, A. et al. TGFα shedding assay: an accurate and versatile method for detecting GPCR activation. *Nat. Methods* **9**, 1021–1029 (2012).
24. Bumbak, F. et al. Stabilization of pre-existing neurotensin receptor conformational states by β-arrestin-1 and the biased allosteric modulator ML314. *Nat. Commun.* **14**, 3328 (2023).
25. Wan, Q. et al. Mini G protein probes for active G protein-coupled receptors (GPCRs) in live cells. *J. Biol. Chem.* **293**, 7466–7473 (2018).
26. Gurevich, V. V. & Gurevich, E. V. GPCR signaling regulation: the role of GRKs and arrestins. *Front. Pharmacol.* **10**, 125 (2019).
27. O'Hayre, M. et al. Genetic evidence that β-arrestins are dispensable for the initiation of β_2-adrenergic receptor signaling to ERK. *Sci. Signal.* **10**, eaal3395 (2017).
28. Duan, J. et al. GPCR activation and GRK2 assembly by a biased intracellular agonist. *Nature* **620**, 676–681 (2023).
29. Papasergi-Scott, M. M. et al. Time-resolved cryo-EM of G-protein activation by a GPCR. *Nature* **629**, 1182–1191 (2024).
30. Vogt, H. et al. Development of a fluorescent ligand for the intracellular allosteric binding site of the neurotensin receptor 1. *ACS Pharmacol. Transl. Sci.* **7**, 1533–1545 (2024).
31. Vadnie, C. A. et al. Activation of neurotensin receptor type 1 attenuates locomotor activity. *Neuropharmacology* **85**, 482–492 (2014).
32. Suratman, S. et al. Impact of species variability and 'probe-dependence' on the detection and in vivo validation of allosteric modulation at the M_4 muscarinic acetylcholine receptor. *Br. J. Pharmacol.* **162**, 1659–1670 (2011).
33. Keov, P., Sexton, P. M. & Christopoulos, A. Allosteric modulation of G protein-coupled receptors: a pharmacological perspective. *Neuropharmacology* **60**, 24–35 (2011).
34. Martin, G. E., Bacino, C. B. & Papp, N. L. Hypothermia elicited by the intracerebral microinjection of neurotensin. *Peptides* **1**, 333–339 (1980).
35. Erwin, V. G. & Su, N. C. Neurotensin and ethanol interactions on hypothermia and locomotor activity in LS and SS mice. *Alcohol Clin. Exp. Res.* **13**, 91–94 (1989).
36. Goupil, E. et al. A novel biased allosteric compound inhibitor of parturition selectively impedes the prostaglandin F2α-mediated Rho/ROCK signaling pathway. *J. Biol. Chem.* **285**, 25624–25636 (2010).
37. Makita, N. et al. An acquired hypocalciuric hypercalcemia autoantibody induces allosteric transition among active human Ca-sensing receptor conformations. *Proc. Natl Acad. Sci. USA* **104**, 5443–5448 (2007).
38. Tateyama, M. & Kubo, Y. Dual signaling is differentially activated by different active states of the metabotropic glutamate receptor 1α. *Proc. Natl Acad. Sci. USA* **103**, 1124–1128 (2006).
39. Eiger, D. S., Hicks, C., Gardner, J., Pham, U. & Rajagopal, S. Location bias: a "hidden variable" in GPCR pharmacology. *Bioessays* **45**, e2300123 (2023).
40. Tennakoon, M. et al. Subtype-dependent regulation of Gβγ signalling. *Cell. Signal.* **82**, 109947 (2021).
41. Goedert, M., Pinnock, R. D., Downes, C. P., Mantyh, P. W. & Emson, P. C. Neurotensin stimulates inositol phospholipid hydrolysis in rat brain slices. *Brain Res.* **323**, 193–197 (1984).
42. Najimi, M., Gailly, P., Maloteaux, J. M. & Hermans, E. Distinct regions of C-terminus of the high affinity neurotensin receptor mediate the functional coupling with pertussis toxin sensitive and insensitive G-proteins. *FEBS Lett.* **512**, 329–333 (2002).
43. Yamada, M., Yamada, M., Watson, M. A. & Richelson, E. Neurotensin stimulates cyclic AMP formation in CHO-rNTR-10 cells expressing the cloned rat neurotensin receptor. *Eur. J. Pharmacol.* **244**, 99–101 (1993).
44. Skrzydelski, D. et al. Differential involvement of intracellular domains of the rat NTS1 neurotensin receptor in coupling to G proteins: a molecular basis for agonist-directed trafficking of receptor stimulus. *Mol. Pharmacol.* **64**, 421–429 (2003).
45. Shi, W. X. & Bunney, B. S. Roles of intracellular cAMP and protein kinase A in the actions of dopamine and neurotensin on midbrain dopamine neurons. *J. Neurosci.* **12**, 2433–2438 (1992).
46. Zhang, J. F., Mehta, S. & Zhang, J. Signaling microdomains in the spotlight: visualizing compartmentalized signaling using genetically encoded fluorescent biosensors. *Annu. Rev. Pharmacol. Toxicol.* **61**, 587–608 (2021).
47. Hedderich, J. B. et al. The pocketome of G-protein-coupled receptors reveals previously untargeted allosteric sites. *Nat. Commun.* **13**, 2567 (2022).
48. Zhang, M., Lan, X., Li, X. & Lu, S. Pharmacologically targeting intracellular allosteric sites of GPCRs for drug discovery. *Drug Discov. Today* **28**, 103803 (2023).
49. Mafi, A., Kim, S. K. & Goddard, W. A. 3rd The mechanism for ligand activation of the GPCR–G protein complex. *Proc. Natl Acad. Sci. USA* **119**, e2110085119 (2022).
50. Peter, S. et al. Comparative study of allosteric GPCR binding sites and their ligandability potential. *J. Chem. Inf. Model.* **64**, 8176–8192 (2024).
51. Kobayashi, K. et al. Class B1 GPCR activation by an intracellular agonist. *Nature* **618**, 1085–1093 (2023).
52. Lees, J. A. et al. An inverse agonist of orphan receptor GPR61 acts by a G protein-competitive allosteric mechanism. *Nat. Commun.* **14**, 5938 (2023).
53. Paxinos, G. and Franklin, K. B. J. *The Mouse Brain in Stereotaxic Coordinates* 2nd edn (Academic Press, 2001).

Methods

Cell lines

HEK293T/17 (CRL-11268, RRID: CVCL_1926) cells were obtained from the American Type Culture Collection (ATCC). G-protein-deficient HEK293 cells (Δ*GNAS*, Δ*GNAL*, Δ*GNAQ*, Δ*GNA11*, Δ*GNA12* and Δ*GNA13*, HEK293 clone 38 (ref. 54) and β-arrestin 1/2-deficient HEK293 cells (Δ*ARRB1* and Δ*ARRB2*; also known as arrestin 2 and arrestin 3, respectively, HEK293 clone 4 (ref. 27)) have been previously described. All cells were cultured in Dulbecco's Modified Eagle Medium (DMEM) with 10% fetal bovine serum (FBS) (Invitrogen, CX30346) and 1× antibiotic antimycotic solution (100 units ml^{-1} penicillin, 100 μg ml^{-1} streptomycin and 250 ng ml^{-1} amphotericin B; Thermo Fisher Scientific, 15240062). Cells were grown exponentially in an incubator at 37 °C under 5% CO_2 and subcultured at ratios of 1:2–1:10 every two to four days using 0.05% trypsin-EDTA (Thermo Fisher Scientific, 25300120).

Chemicals

All chemicals were obtained from MilliporeSigma unless otherwise noted. SBI-0654553 HCl (abbreviated as SBI-553) was synthesized by the Conrad Prebys Center for Chemical Genomics at the Sanford Burnham Prebys Medical Discovery Institute. Coelenterazine *h* and coelenterazine 400a were obtained from Cayman Chemical. For receptor signalling assessments, NT (Sigma, N6383) and PD149163 (Sigma, PZ0175) were maintained as 2 mM stock in 80% glycerol. SBI-553 and SR142948A (Sigma, SML0015) were maintained as 50 mM stocks in dimethyl sulfoxide (DMSO). SBI-0654553 analogues were synthesized using previously published methods[3]. Derivates were maintained as 50, 25 or 12.5 mM stocks in DMSO, as solubility permitted. For in vivo studies, SBI-553 and SBI-593 were freshly prepared from powdered stocks. When applicable, doses and concentrations were calculated from the formula weight of the compound salts and adjusted for fractional anhydrous base weight.

Recombinant DNA plasmids

The 3×HA-NTSR1 plasmid consists of N-terminal 3×HA-tagged WT human NTSR1 cloned into the pcDNA3.1(+) vector (Invitrogen, Thermo Fisher Scientific) at KpnI (5′) and XbaI (3′). This construct was purchased from the University of Missouri (cDNA Bank, NTSR10TN00). TRUPATH was a gift from B. Roth (Addgene kit 1000000163). The pcDNA3.1Zeo(−) vector was acquired from Invitrogen. The mVenus-β-arrestin 1 (human) and mVenus-β-arrestin 2 (human) plasmids consist of human β-arrestin 1 (cDNA Bank, ARRB100002) or human β-arrestin 2 (cDNA Bank, ARRB200001) cloned in frame, through restriction cloning, into a pcDNA3.1 plasmid that contained the mVenus sequence in the N-terminal position. The G_q–Rluc8 single-point mutants (corresponding G_q residues: V359Y, N357G, Y356C and L351N) were obtained by single-nucleotide mutagenesis using the QuikChange II XL kit (Agilent Technologies), following the manufacturer's specifications. The mVenus-tagged mini-G_o was generated by G-block synthesis of the reported mini-G_o sequence[55] and in-frame restriction cloning into the same backbone as the rest of the mini-G constructs. The 5 and 13 C-terminal substitutions in the TRUPATH Gα subunits were performed by oligonucleotide synthesis and annealing, followed by in-frame restriction cloning. Cloning of β-arrestin and G protein sensors was performed by the University of Minnesota Viral Vector and Cloning Core and validated through Sanger sequencing.

BRET2 G protein activation assays

In the BRET2-based TRUPATH platform[22], G protein activation results in a decrease in BRET between an Rluc8-tagged Gα and a GFP2-tagged Gγ protein. For visualization purposes, we plotted transformed (−Δ net BRET) data, such that G protein activation produces upward sloping curves. Curve height is a function of both the number of Gα–Gβγ complexes dissociating and the relative proximity of the Rluc8 and GFP2 tags. Because tag location differs among the Gα proteins and distinct γ subfamily members are used for each Gα protein, maximal changes in BRET are expected to differ among the Gα sensors. We retain the original BRET values on these curves to preserve information on sensor dynamic range. On day 1, HEK293T cells were plated in 6-well plates (750,000 per well) in DMEM containing 10% FBS and 1% 1× antibiotic antimycotic solution. On day 2, cells were transiently transfected with NTSR1 (200 ng per well), Gβ1 or Gβ3 (100 ng per well), GFP2-tagged Gγ9, Gγ8, Gγ13 or Gγ1 (100 ng per well) and the Gα of interest using a standard calcium phosphate transfection protocol, and the pairings of Gα, Gβ and Gγ subunits as described previously[22] For mutant G proteins, the preferred βγ combination for the G protein base was maintained. A summary of βγ selections is provided in Supplementary Table 13. This produces a receptor:Gα:Gβ:Gγ ratio of 2:1:1:1. On day 3, cells were plated (25,000 cells per well) onto poly-D-lysine (PDK)-coated (100 ng ml^{-1}), clear-bottom, white-walled 96-well plates in Opti-MEM containing 2% FBS and 1% 1× antibiotic antimycotic solution. On day 4, cells were incubated in 70 or 80 μl per well Hanks' balanced salt solution (HBSS) containing calcium and magnesium and 20 mM HEPES for five to six hours before treatment. Cells receiving an SBI-553 or SR142948A pretreatment were incubated in 70 μl per well of HBSS containing 20 mM HEPES. Cells not receiving any pretreatment were incubated in 80 μl per well of HBSS plus 20 mM HEPES. SR142948A was freshly prepared in HBSS from a 50 mM DMSO stock. The 10× NT and PD149163 were freshly prepared in HBSS from 2 mM 80% glycerol (NTS, PD149163) stocks, and 10× SBI-553 was freshly prepared in HBSS with 5% 2-hydroxylpropyl-β-cyclodextrin (HP-β-CD, Tokyo Chemical Industry) from a 50 mM DMSO stock. For SAR studies, 10× SBI-553 and all derivatives were freshly prepared in 30% HP-β-CD from 50, 25 or 12.5 mM DMSO stocks. A white vinyl sticker was placed on the bottom of the plate. For room-temperature studies, plates were allowed to cool for 10 min until they reached approximately 25 °C. Ten microlitres of 10× SBI-553, SR142948A or SBI-553 derivative pretreatments were added during the 10-min cooling period, a total of 20 min before reading. For studies at 35 °C, treatments were incubated at temperature. Ten microlitres of 10× NTS, PD149163, SBI-553 or SR142948A treatments were added 10 min before reading. Ten microlitres per well of a 10× concentration of coelenterazine 400a (final concentration around 7.5 μM, Cayman Chemical) was added 5 min before reading. After treatment with coelenterazine 400a, plates were protected from light. Plates were read with a Tecan SparkCyto Microplate reader at room temperature (25 °C) or 35 °C in ambient air every 5 min for 20 min. BRET2 ratios were computed as the ratio of GFP2 emission to Rluc8 emission. The Δ net BRET ratio was calculated by subtracting the stimulated GFP2/Rluc8 ratios from control GFP2/Rluc8 ratios for each read. The minimum Δ net BRET ratio over time was averaged within treatments and combined between experiments. Data are presented as negative mean Δ net BRET ratio ± s.e.m. from at least three independent experiments.

BRET1 β-arrestin recruitment assays

Recruitment of mVenus-tagged human β-arrestin 1 and human β-arrestin 2 to *Renilla* luciferase (Rluc8)-tagged NTSR1 was assessed in HEK293T cells using a BRET assay, as described[4]. Previous studies evaluating NTSR1 β-arrestin agonism have used bovine or rodent β-arrestin constructs[4,5]. To assess recruitment of the human β-arrestins, the following procedure was used. On day 1, HEK293T cells were plated in 6-well plates (750,000 per well) in growth medium. On day 2, cells were transiently transfected with Rluc8-tagged NTSR1 (100 ng per well), Venus-tagged β-arrestin 2 or Venus-tagged β-arrestin 1 (1.4 μg per well), and pcDNA3.1 (1.5 μg per well) using a standard calcium phosphate transfection protocol. To maximize assay sensitivity, with the exception of the NT combination studies in Fig. 2, transfections also included 500 ng GRK2. On day 3, cells were plated onto PDK-coated (100 ng ml^{-1}), clear-bottom, white-walled 96-well plates (40,000 cells per well) in Opti-MEM containing 2% FBS and 1× antibiotic antimycotic solution.

On day 4, cells were incubated in 70 or 80 µl per well HBSS containing calcium and magnesium and 20 mM HEPES for five to six hours before treatment. Cells receiving an SBI-553 or SR142948A pretreatment were incubated in 70 µl per well of HBSS containing 20 mM HEPES. Cells not receiving a pretreatment were incubated in 80 µl per well of HBSS plus 20 mM HEPES. The 10× NT and PD149163 were freshly prepared in HBSS from 2 mM 80% glycerol (NT, PD149163) stocks, and 10× SBI-553 was freshly prepared in HBSS with 5% HP-β-CD from a 50 mM DMSO stock. For SAR studies, 10× SBI-553 and all derivatives were freshly prepared in 30% HP-β-CD from 50, 25 or 12.5 mM DMSO stocks. For compound combination studies, cells were pretreated with 10 µl of 10× SBI-553, SR142948A or vehicle pretreatments 15 min before reading. Ten microlitres per well of a 10× concentration of coelenterazine *h* (final concentration 4.7 µM; Cayman Chemical) was added 10 min before reading, followed by treatment with 10 µl of 10× NT 5 min before reading. Cells receiving no pretreatment received 10 µl of 10× NT, PD149163, SBI-553 and SR142948A treatments 10 min before reading and 10× coelenterazine *h* 5 min before reading. For experiments in Figs. 1 and 2, plates were maintained and read at room temperature. For the temperature studies, time-course studies and analogue screening and characterization in Extended Data Figs. 2, 3 and 6–8, plates were maintained at 35 °C during treatment and reading. A white vinyl sticker was placed on the bottom of each plate. Plates were read with a CLARIOstar Plus microplate reader (BMG Labtech) set at 25 °C or 35 °C at 10, 15, 20, 25, 30 and 35 min after treatment. BRET1 ratios were computed as the ratio of Venus emission to Rluc8 emission. The Δ net BRET ratio was calculated by subtracting the stimulated Venus/Rluc8 ratios from control Venus/Rluc8 ratios for each read. The maximum Δ net BRET ratio over time was averaged within treatments and combined between experiments. Data are presented as mean Δ net BRET ratio ± s.e.m. from at least three independent experiments.

TGFα shedding assays of G protein activation

TGFα shedding assays of G protein activation were performed as originally presented[23], with previously described modifications[4,56]. These modifications included using G-protein-deficient (Δ*GNAS*, Δ*GNAL*, Δ*GNAQ*, Δ*GNA11*, Δ*GNA12* and Δ*GNA13*) HEK293 cells[54] and the fluorescent substrate 4-methylumbelliferyl phosphate (4-MUP), at a working concentration of 1 mM per well, instead of p-nitrophenyl phosphate (p-NPP). On day 1, G-protein-deficient HEK293 cells were plated in 6-well plates (750,000 per well) in growth medium. On day 2, expression vectors were transiently transfected in HEK293 cells using Lipofectamine 2000 (Invitrogen; 8 µl per well in a six-well plate). Expression vectors included 1.875 µg AP-TGFα, 750 ng HA-tagged NTSR1 and 350 ng of Gα protein. On day 3, transfected cells were detached with a brief rinse (1 ml, around 30 s) of phosphate-buffered saline (PBS) followed by 0.5 ml per well of 0.05% trypsin-EDTA (Gibco). The cell suspension was pelleted by centrifugation (200*g*, 5 min), followed by a resuspension in 3 ml HBSS containing 5 mM HEPES (pH 7.4) and a 10-min incubation at room temperature. Cells were again centrifuged (200*g*, 5 min) and resuspended in 4 ml HBSS containing 5 mM HEPES (pH 7.4). The resuspended cells were plated in 80 µl per well in a 96-well plate and placed in an incubator at 37 °C with 5% CO_2. After a 30-min incubation, cells were treated with 10 µl vehicle (HBSS), 10× final concentrations of SR142948A or SBI compounds and incubated at 37 °C for 20 min. For preparation of 10× stocks, SBI compounds and SR142938A were diluted directly from 1–10 mM DMSO stocks into HBSS. The final concentration of DMSO did not exceed 0.4%. After a 20-min incubation with SBI compounds, cells were treated with 10 µl of 10× concentration of NT and incubated at 37 °C for one hour. For inhibition studies, 10 nM NT was used for the G_q, $G_{i1/2}$ and G_{12} constructs, and 100 nM was used for the G_o construct; these concentrations were selected to elicit maximal NT-induced shedding. Plates were centrifuged (190*g*, 2 min) and conditioned medium (80 µl) was transferred into a new 96-well plate. After a 20-min incubation at room temperature, 2 mM 4-MUP-containing solution was added (80 µl per well) to both the conditioned medium and the cell plate. Alkaline phosphatase activity was measured using a CLARIOstar Plus microplate reader set to 25 °C. Data were collected before and after a one-hour incubation at 37 °C. Excitation was set at 360 nm (±10 nm) and emission at 450 nm (±15 nm). TGFα shedding activity was calculated by dividing the amount of phosphatase activity present in the conditioned medium by the amount present on the cells plus the conditioned medium. All values were standardized to background shedding activity.

Mini-G protein recruitment assays

Mini-G proteins have a truncated N terminus and contain a mutation that uncouples GPCR binding from nucleotide release, allowing them to form more stable associations with GPCRs than do unmodified G proteins[25,55]; these associations are amenable to monitoring by BRET. The recruitment of Venus-tagged mini-G proteins[25] to Rluc8-tagged NTSR1 was assessed by BRET. Note that although mini-G_o and mini-G_{12} were derived from their full-length versions, the mini-G_q and mini-G_{i1} constructs were derived from the G_s backbone with substitution of the α5 helix[25,55]. To assess recruitment, on day 1, HEK293T cells were plated in 6-well plates (750,000 per well) in growth medium. On day 2, cells were transiently transfected with Rluc8-tagged NTSR1 (100 ng per well), a Venus-tagged mini-G protein and pcDNA3.1 (1.5 µg per well or 2.65 µg per well) using a standard calcium phosphate transfection protocol. Cells transfected with a Venus-tagged mini-G_q or mini-G_{i1} received 250 ng per well. Cells transfected with a Venus-tagged mini-G_{12}, mini-G_s or mini-G_o received 1.5 µg per well. On day 3, cells were plated onto PDK-coated (100 ng ml^{-1}), clear-bottom, white-walled 96-well plates (40,000 cells per well) in Opti-MEM containing 2% FBS and 1× antibiotic antimycotic solution. On day 4, cells were incubated in 70 or 80 µl per well HBSS containing calcium and magnesium and 20 mM HEPES for three to four hours before treatment. Cells receiving an SBI-553, PD149163 or SR142948A pretreatment were incubated in 70 µl per well of HBSS containing 20 mM HEPES. Cells not receiving any pretreatment were incubated in 80 µl per well of HBSS plus 20 mM HEPES. Cells were pretreated with 10 µl of 10× concentrations of SBI compounds, SR142948A, PD149163 or vehicle (5% or 30% HP-β-CD) 20 min before reading. Cells were then treated with vehicle (HBSS) or 100 nM NT 10 min before reading. Finally, cells were treated with 10 µl per well of a 10× concentration of coelenterazine *h* (final concentration 4.7 µM) 5 min before reading. Plates were read on a CLARIOstar Plus microplate reader set at 25 °C at 5, 10, 15 and 30 min after treatment. Mini-G protein recruitment was calculated by subtracting the stimulated Venus/Rluc8 ratios from control Venus/Rluc8 ratios for each read (Δ net BRET).

Western blot analysis

β-Arrestins 1 and 2 were detected by Western blot. On day 1, HEK293T and β-arrestin 1/2-null HEK293 cells were plated at 750,000 cells per well onto 6-well plates. On day 2, cells were lysed on ice in 2× sample buffer. Whole-cell lysates were sonicated and then analysed for expression of β-arrestins 1 and 2. Cell protein samples (10 µl) were resolved on 10% SDS–polyacrylamide gels (NuPAGE, Bis-Tris; Thermo Fisher Scientific) and transferred to nitrocellulose membranes (0.45 µm pore size; Thermo Fisher Scientific). The membrane was rinsed with Tris-buffered saline (TBS; Li-Cor Biosciences) and then stained with Ponceau S solution (Sigma-Aldrich, 6226-79-5) to visualize protein loading. Membranes were rinsed three times with 50% TBS containing 0.1% Tween-20 (v/v; TBST) and incubated in Odyssey Blocking Buffer for one hour at room temperature. Blocked membranes were incubated overnight at 4 °C with rabbit anti-β-arrestin 1/2 (Cell Signaling Technology, 4674, RRID: AB_10547883) in 50% blocking buffer and 50% TBST at a 1:1,000 dilution. Membranes were washed with TBST before and after incubation with infrared secondary antibodies Alexa Fluor goat anti-rabbit 680 (Invitrogen, A-21109, RRID: AB_2535758) at a 1:5,000

dilution for one hour at room temperature. Membranes were imaged on a LI-COR Biosciences Odyssey imaging system.

Optimization of the structure of the NT–NTSR1–SBI-553–G_{oA} complex for modelling

The cryo-electron microscopy (cryo-EM) structure of NTSR1 bound to SBI-553 and G_o (PDB: 8FN0) was used at the starting point for modelling. Structure preparation was performed with Maestro (Schrödinger). VDW clashes were removed by constrained minimization using the OPLS4 force field. A full conformational analysis was performed with the conformational ensemble generated by MOE (Chemical Computing Group) and minimization using density functional theory calculations (Gaussian, ωb97XD/6-311+G** functional). The SBI-553 piperidine preferred a chair conformation over the twist boat by more than 3.1 kcal mol^{-1}. As a result, the SBI-553 conformation from PDB: 8JPB was substituted into the model by rigid superposition of the two SBI-553 conformations followed by a second constrained minimization of the minor clashes resulting from this replacement. Molecular mechanics calculations (minimization and molecular dynamics) with multiple force fields orient the fluorine on SBI-553's cyclopropyl group perpendicular to the quinazoline ring. To investigate this orientation, a rotational analysis was performed on SBI-553, SBI-342 and SBI-593 at 10° increments about the quinazoline–cyclopropane C–C bond with full minimization using ωb97XD/6-311+G**. For each molecule, there was a strong preference (2.5 to 3.2 kcal mol^{-1}) for the conformation reported in a previous study[5] in which the substituent on the cyclopropane (F for SBI-553, CH_3 for SBI-342 and H for SBI-593) is in the plane of the quinazoline and pointed away from the appended piperidine. Subsequent protein minimizations and molecular dynamics simulations used explicit constraints to maintain desired small-molecule conformations.

G protein homology modelling

Homology models of each G protein were built with MOE (v.2022.02, Chemical Computing Group), with the conformation of each mutated side chain optimized individually using MOE's Amber 10:EHT force field. Models of G_q conformations required building the NTSR1 H1/H2 loop absent in PDB: 8FN0. This loop is resolved in the PDB: 6OS9 structure, so the missing residues were concatenated onto PDB: 8FN0 using the homology model application in MOE. Minimization of the protein complexes containing SBI-342 and SBI-593 used the OPLS4 force field in Maestro (v.14.1.138, Schrödinger).

Molecular dynamics simulations

Molecular dynamics simulations with G_q and SBI-593 were done with Desmond using the Schrödinger suite (v.14.3.129 and v.13.7.125). Standard protein preparation included building the G87–E92 loop of mini-G_q. SBI-593 was superimposed onto SBI-553, and G_q was mapped onto G_o from PDB: 8FN0. The conformation of each side chain of G_q-H5 was independently sampled and quaternary (NTSR1, G_q, NT and SBI-553) complex minimized. Where side chains interacted with each other, multiple side-chain combinations were assessed and their energies compared. The side-chain rotamers were well-sampled during the dynamics runs. Dynamics set-up included explicit water, manually placed 1-palmitoyl-2-oleoyl-*sn*-glycero-3-phosphocholine (POPC) membrane, 0.15 N NaCl and a constraint on cyclopropyl rotation. Six discrete simulations were performed (three 100 ns and three 300 ns) using the NPγT ensemble, OPLS5 force field and TIP3P water model (300 K). Equilibration used a 100-ps NVT ensemble simulation with Brownian dynamics at 10 K, a 12-ps NVT ensemble simulation with a Langevin thermostat at 10 K, two constrained 12-ps NPT simulations using a Langevin thermostat and barostat at 1 atm at 10 K then 300 K, and a 24-ps NPγT equilibration using a Langevin thermostat and barostat at 300 K and 1 atm. Membrane relaxation used a 1-ps Nose–Hoover chain thermostat and a 2-ps Martyna–Tobias–Klein barostat. Root mean square deviation (RMSD) was measured for the Cα carbons, and side-chain movement was monitored to ensure adequate sampling of conformational space. Once the complex stabilized to a consistent Cα RMSD, 20–25 frames from each run were selected from periods of the greatest RMSD stability. Each complex was minimized in Maestro, in which conformations, orientations and energies were compared.

Mice

All mouse studies were performed in accordance with the National Institutes of Health Guidelines for Animal Care and Use of Laboratory Animals and with approved animal protocols from the University of Minnesota University Animal Care and Use Committee. The mice studied included: C57BL/6J mice (Jackson Laboratory, 000664), global *Ntsr1*$^{-/-}$ mice (B6.129P2-Ntsr1tm1Dgen/J, Deltagen, Jackson Laboratory strain 005826), β-arrestin 2-knockout (*Arrb2*$^{-/-}$) mice[57] and their respective WT littermates. All mouse lines were backcrossed onto a C57BL/6J genetic background for at least ten generations before use. At the start of the study, all mice were adults. Mice were 8–20 weeks old, weighed 19–30 g, and were age-matched across experimental groups. Experiments included both male and female mice, and experimental groups were sex-matched. *Ntsr1*$^{-/-}$ and *Arrb2*$^{-/-}$ mice for experimental use were exclusively generated by *Ntsr1*$^{+/-}$ × *Ntsr1*$^{+/-}$ or *Arrb2*$^{+/-}$ × *Arrb2*$^{+/-}$ breeding, such that littermate WT mice could serve as controls. Littermates of the same sex and genotype were randomly assigned to experimental groups. Mice for systemic PD149163-induced hypothermia studies were group housed in conventional cages with Teklad irradiated corncob bedding (Inotiv) and Enviro-Dri nesting material (Fibercore) and maintained on a 14-h–10-h light–dark cycle. Mice for local NAc injection studies were singly housed after implantation of intracranial cannulas in conventional cages with Teklad irradiated corncob bedding (Inotiv) and Enviro-Dri nesting material (Fibercore), and maintained on a 14-h–10-h light–dark cycle. Experiments began at the start of the light cycle (within three hours of the light cycling beginning). Tap water and standard laboratory chow were supplied ad libitum, except during testing.

Assessments of core body temperature

Core body temperatures were measured using a rectal probe thermometer for mice (Thermalert Model TH-8, Physitemp Instruments), as described[4]. Core body temperatures were recorded from age-matched male and female *Ntsr1*$^{-/-}$ and WT mice before treatment (time 0) and 30, 60, 90, 120 and 300-min after treatment. Mice were gently restrained during the procedure and acclimated to this process during baselining. For single-compound dosing studies, baseline temperatures were recorded, and mice received either PD149163 (0.03–1 mg kg^{-1}) or PD149163's vehicle (physiological saline). All treatments were administered i.p. in a volume of 10 ml kg^{-1}. For systemic multiple-compound dosing studies, mice received SBI-553 (12 mg kg^{-1}, i.p.) or its vehicle (5% cyclodextrin) or SBI-593 (12 mg kg^{-1}, i.p.) or its vehicle (20% DMSO, 5% Tween-80) before the start of the study (−45 min). After temperature recording at time 0, mice received PD149163 (0.15 mg kg^{-1}) in volumes of 10 µl per kg i.p.

Intracranial cannulation and local NAc injections

Local NAc microinjections were accomplished after bilateral guide cannula placement in *Ntsr1*$^{-/-}$ mice and their WT littermates, C57BL/6J mice. Cannulas were acquired from Plastics One (bilateral guide: 2.0 mm spacing, 26G, 4 mm below pedestal; bilateral internal: 2.0 mm spacing, 33G, 0.5 mm projection; bilateral dummy: 2.0 mm spacing, 0.008″/0.2 mm, 0 mm projection). Bilateral guide cannulas were inserted into the NAc at +1.3 mm AP with 2.0-mm spacing (±1.0 mm mediolateral (ML)) and −4.5 mm dorsoventral (DV) and fixed to the skull with dental cement. Mice were singly housed after surgery and allowed to recover for at least seven days. After recovery, compounds were injected bilaterally using an automated syringe pump (Harvard Apparatus). SBI-553 (molecular weight 450 g mol^{-1}) was dissolved in 1% (v/v) DMSO and 20% (v/v) HP-β-CD at 74.07 mM. One hundred micrograms of SBI-553 in 3 µl was injected per side at a rate of 0.2 µl per min. SBI-593 (molecular weight

458 g mol^{-1}) was dissolved in 80% (v/v) *N*,*N*-dimethylacetamide, 10% (v/v) Tween-80 and 10% (v/v) UltraPure distilled water at 72.7 mM. One hundred micrograms of SBI-593 in 3 µl was injected per side at a rate of 0.2 µl per min. After local injection of SBI compounds, mice were placed in their home cages for one hour before intra-NAc administration of PD149163. PD149163 (molecular weight 943.91 g mol^{-1}) was diluted from a stock concentration of 2 mM in 80% glycerol to 10 or 100 µM in separate SBI compound or vehicle preparations, and 18.9, 1.89 or 0.189 ng PD149163 in 0.2 µl was injected per side at a rate of 0.2 µl per min. The PD149163 dose used was 18.9 ng in the WT versus *Ntsr1*$^{-/-}$ experiments, 1.89 ng in the 100-µg SBI-553 experiments and 0.189 ng in the 10-µg SBI pretreatment experiments. The GRK2/3 inhibitor Compound 101 (Hello Bio) was diluted in vehicle (10% (v/v) DMSO and 20% (v/v) hydroxypropyl cyclodextrin) from a stock concentration of 20 mM in DMSO to 1.99 mM and 0.5 µg in 0.5 µl was injected per side at a rate of 0.4 µl per min one hour before the injection of 1.89 ng PD149163. This Compound 101 dose and preparation was previously shown to inhibit GRK2/3-mediated effects after intracranial delivery in mice[57]. After local injection of PD149163, body temperature was monitored every 30–60 min for 8 h. For all experiments, mice were randomly assigned to treatment groups for no more than two experiments, separated by a minimum of seven days. Cannula placements were verified by ink injection. After the experiment, 0.5 µl India ink (1:20 (v/v) saline) was injected at a flow rate of 0.5 µl per min to visualize the observed injection site. Injection sites were identified using anatomical makers and documented on a coronal mouse brain atlas[53]. Mice were anaesthetized with isoflurane and brains were collected one hour after ink microinjection. Brains were sliced in 250-µm sections using a vibratome (VT1000S, Leica).

Statistical analysis

All data are represented as mean ± s.e.m., unless otherwise indicated. Data were analysed and plotted using the software GraphPad Prism v.10.1.2. Information on curve fitting, statistical tests and *n* numbers are provided in Supplementary Tables 1–6. In Supplementary Tables 1–6, *n* represents the number of biological replicates. All data represent the average of at least three biological replicates from three independent experiments. Cell-based experiments included two or three technical replicates for every condition. A *P* value of less than 0.05 was accepted as statistically significant.

Figure illustrations

Method and concept figure illustrations were created using BioRender. Images of NTSR1 and G protein structures were created in ChimeraX (UCSF, v.1.6). Cannula placements are presented on Paxinos and Franklin's 'The Mouse Brain In Stereotaxic Coordinates'[53].

Reporting summary

Further information on research design is available in the Nature Portfolio Reporting Summary linked to this article.

Data availability

The data that support the findings of this study are available in the Supplementary Information and have been deposited in the Harvard Dataverse under https://doi.org/10.7910/DVN/J10DSJ. Additional information and materials are available from the corresponding author on request. Source data are provided with this paper.

54. Grundmann, M. et al. Lack of β-arrestin signaling in the absence of active G proteins. *Nat. Commun.* **9**, 341 (2018).
55. Nehme, R. et al. Mini-G proteins: novel tools for studying GPCRs in their active conformation. *PLoS ONE* **12**, e0175642 (2017).
56. Pack, T. F., Orlen, M. I., Ray, C., Peterson, S. M. & Caron, M. G. The dopamine D_2 receptor can directly recruit and activate GRK2 without G protein activation. *J. Biol. Chem.* **293**, 6161–6171 (2018).
57. Urs, N. M. et al. Distinct cortical and striatal actions of a β-arrestin-biased dopamine D2 receptor ligand reveal unique antipsychotic-like properties. *Proc. Natl Acad. Sci. USA* **113**, E8178–E8186 (2016).

Acknowledgements TRUPATH was a gift from B. Roth (Addgene kit 1000000163). We thank B. Roth and B. Krumm for sharing mini-G protein pcDNA constructs; O. Rainwater and S. Serres for maintaining the *Ntsr1*$^{-/-}$, *Arrb2*$^{-/-}$ and C57BL/6J mouse colonies; C. Liu for sharing the rat *Ntsr1* pcDNA construct; N. Xiong, L. Iskander, N. Clark and F. Porkka for technical assistance; M. D. Bartberger for consulting on computational chemistry approaches; and D. O'Keefe for critical reading of this manuscript and comments. This work was supported, in part, by NIH/NIDA R00 DA048970 (L.M.S.), NIH/NIDA UH3 DA050316 (M.R.J., L.S.B., L.M.S. and S.H.O.), NIH/NIDA R01 DA061773 (L.M.S. and S.H.O.), NIH/NIDA F31 DA062411 (M.N.M.), DOD W81XWH-22-1-0266-PR211151 (L.S.B. and L.M.S.) and the University of Minnesota Foundation AP-0323-04 (L.M.S.). This work was also supported by the NIH/NIDA P30DA048742-sponsored Viral Innovation Core at the University of Minnesota. A.I. was funded by KAKENHI JP21H05113 and JP24K21281 from the Japan Society for the Promotion of Science (JSPS), JP22ama121038 and JP22zf0127007 from the Japan Agency for Medical Research and Development (AMED) and JPMJFR215T and JPMJMS2023 from the Japan Science and Technology Agency (JST).

Author contributions Study design: L.M.S., S.H.O., E.M.F.d.V., M.N.M., K.L.P., V.L.R., A.R.A., C.L.K. and M.J.S. Obtaining funding: L.M.S., L.S.B., M.R.J. and S.H.O. Data collection: A.R.A., M.N.M., K.L.P., V.L.R., C.L.K., C.R. and N.F. TRUPATH G protein activation: A.R.A., M.N.M., K.L.P., V.L.R., C.L.K., C.R. and L.M.S. β-Arrestin recruitment: A.R.A., M.N.M., K.L.P., V.L.R., C.L.K. and L.M.S. TGFα shedding G protein activation: M.N.M. and C.R. Mini-G recruitment: K.L.P. Western blot analysis: V.L.R. Cloning: E.M.F.d.V. and C.R. Homology modelling: S.H.O., M.J.S. and L.M.S. Molecular dynamics simulations: S.H.O. Mouse body temperature measurements: L.M.S. and M.N.M. Intracranial cannulation and regional brain injections: M.N.M. and L.M.S. Data analysis: M.N.M., K.L.P., A.R.A., V.L.R., S.H.O. and L.M.S. Data interpretation: M.N.M., K.L.P., V.L.R., A.R.A., C.R., A.I., L.S.B., E.M., S.H.O. and L.M.S. Drafting paper: L.M.S., S.H.O., M.N.M., K.L.P. and A.R.A. Revising paper critically for intellectual content: S.H.O., M.N.M., K.L.P., E.M.F.d.V., V.L.R., A.R.A., C.L.K., N.F., C.R., A.I., L.S.B., M.J.S., M.R.J. and L.M.S.

Competing interests US Patent 9,868,707 relating to composition of matter for SBI-553 and its derivatives was issued to the Sanford Burnham Prebys Medical Discovery Institute (SBP) and Duke University, and US Patent 10,118,902 has been issued to SBP. Patent application US20240398806 related to the use of SBI-553 and its derivatives has been filed by Duke University. L.M.S., S.H.O. and M.R.J. are scientific founders of BAM Therapeutics and hold a financial interest in the company. The remaining authors declare no competing interests.

Additional information

Supplementary information The online version contains supplementary material available at https://doi.org/10.1038/s41586-025-09643-2.

Correspondence and requests for materials should be addressed to Lauren M. Slosky.

Peer review information *Nature* thanks John McCorvy, Graeme Milligan and the other, anonymous, reviewer(s) for their contribution to the peer review of this work. Peer reviewer reports are available.

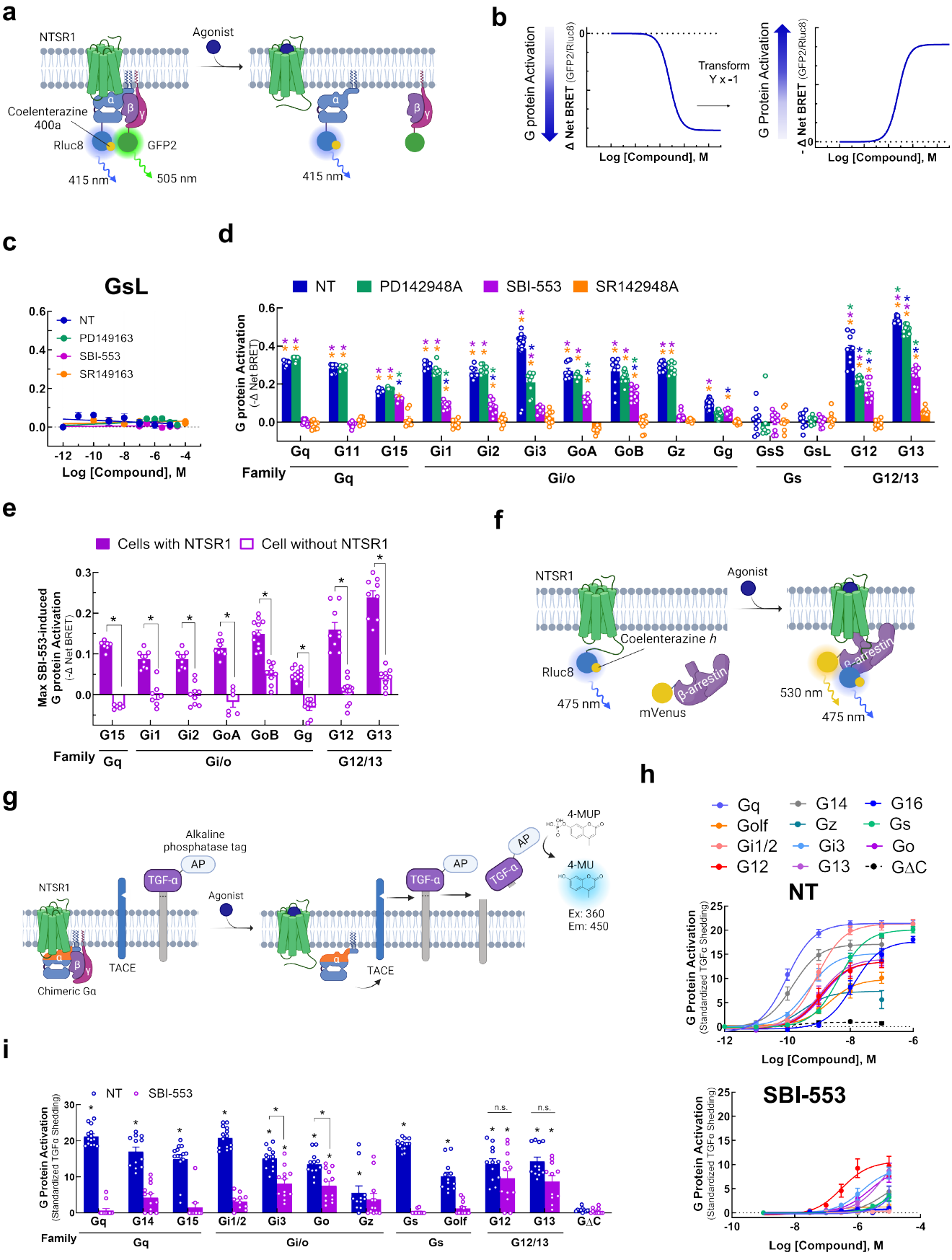

Extended Data Fig. 1 | See next page for caption.

Extended Data Fig. 1 | Assessment of NTSR1 ligand-induced transducer activation. (A) Illustration of BRET2-based TRUPATH assay of G protein activation. **(B)** Depiction of TRUPATH data transformation. G protein activation results in reduced BRET as a BRET donor tagged Gα and a BRET acceptor tagged Gγ subunit dissociate. Curves were inverted such that G protein activation resulted in upward sloping curves. **(C–E)** G protein activation by TRUPATH was assessed following treatment with NT, PD149163, SBI-553, and SR142948A, as described in Fig. 1b. **(C)** For the GsL TRUPATH sensor, activation was not detected. **(D)** Maximal ligand-induced G protein activation in Fig. 1b. Data from n = 4 independent experiments for GoB, Gg, Gs GsS, and β-arrestins and 3 independent experiments for all other transducers, each with technical replicates, were analysed by two-way ANOVA followed by Tukey multiple comparisons tests, $p < 0.0001$. At each G protein, coloured asterisks over the bar indicate the treatments from which that compound significantly (post hoc $p < 0.05$) differed. Treatment vs NT (*, blue), SR142948A (*, orange), PD149163 (*, green), SBI-553(*, magenta). **(E)** Maximal SBI-553-induced G protein activation in cells transiently expressing NTSR1 or an empty control vector. Data from n = 4 independent experiments each with technical replicates were analysed by two-way ANOVA followed by Tukey multiple comparisons tests, $p < 0.0001$. *post hoc $p < 0.05$. **(F)** Illustration of BRET1-based assay for β-arrestin recruitment. **(G)** Illustration of TGFα shedding assay for G protein activation. **(H)** Ligand-induced G protein activation. Data from n = 4 independent experiments each with technical replicates. **(I)** Maximal G protein activation following treatment with NT or SBI-553 presented in panel H. Data were analysed by two-way ANOVA followed by Bonferroni multiple comparisons test, *$p < 0.0001$. *$p < 0.05$ post hoc change vs GΔC, unless otherwise indicated. All data are presented as mean ± s.e.m. For curve parameters and additional information on comparisons, see Supplementary Table 7. Supporting main text Fig. 1. Illustrations in **a**,**f**,**g** created using BioRender (Slosky, L. (2025) https://BioRender.com/cjdt0k0, https://BioRender.com/83xz8on, https://BioRender.com/os8nkwk).

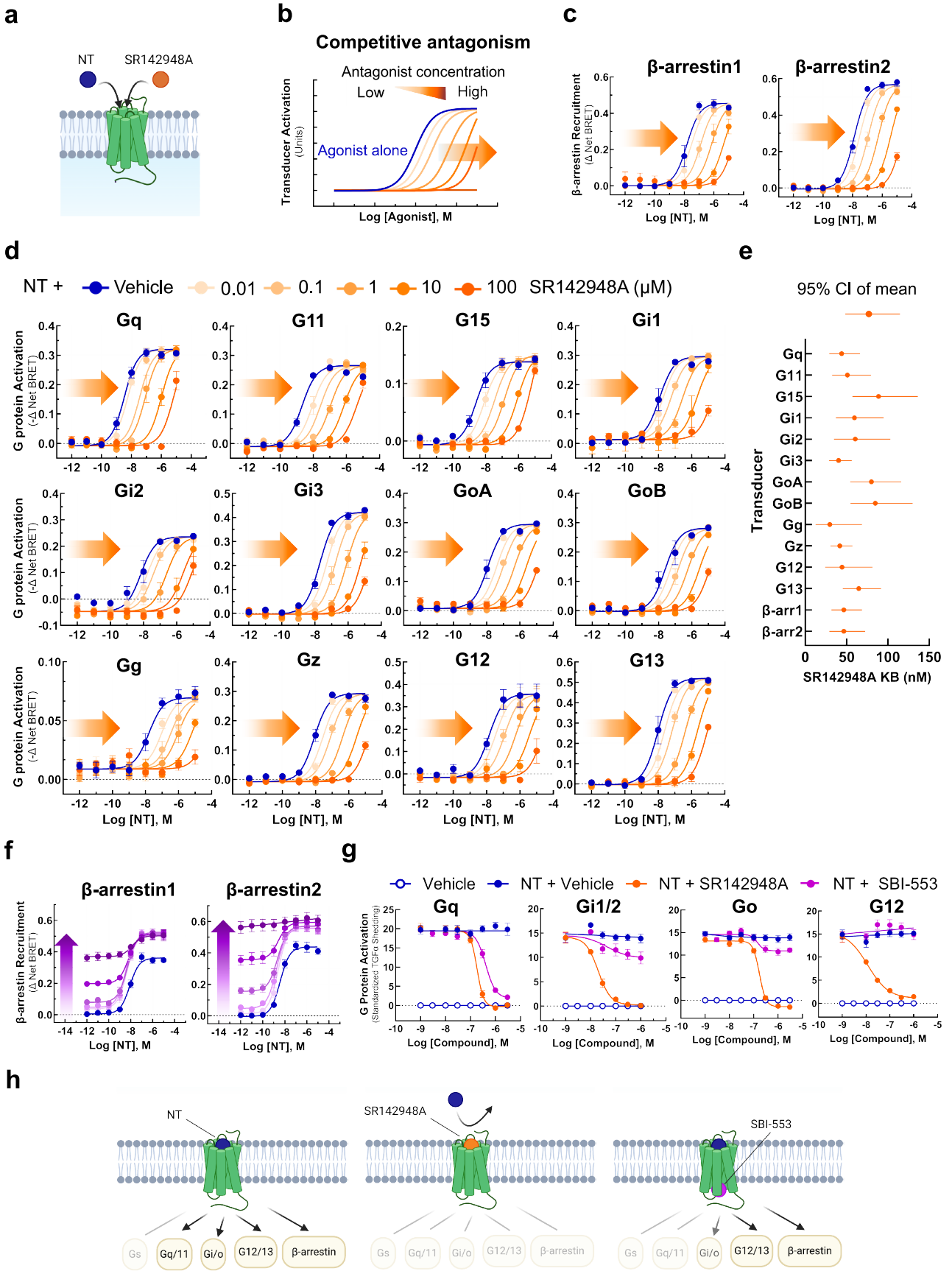

Extended Data Fig. 2 | See next page for caption.

Extended Data Fig. 2 | SR142948A uniformly and competitively antagonizes NT-induced NTSR1 transducer activation. **(A)** Illustration of NT and SR142948A competing to occupy the same binding site on NTSR1. **(B)** Characteristic agonist CRC shifts in the presence of increasing concentrations of a competitive antagonist. **(C)** NT-induced β-arrestin-1/2 recruitment to the NTSR1 was assessed by BRET in the absence and presence of SR142948A. n = 3 independent experiments. **(D)** NT-induced G protein activation was assessed by TRUPATH in the absence and presence of SR142948A. n = 3 independent experiments. **(E)** SR142948A antagonistic potency is comparable across transducers, as evidenced by overlapping K_B 95% confidence intervals (CIs). **(F)** NT-induced human β-arrestin-1/2 recruitment to the NTSR1 in the absence and presence of SBI-553. n = 3 independent experiments. **(G)** Effect of SR142948A and SBI-553 on NT-induced G protein activation, second assay validation. NT-induced G protein activation was assessed by TGFα shedding. NT-induced activation of Gq, Gi1/2, Go, and G12 sensors in the presence of SR142948A, SBI-553, or vehicle. Curves were fitted to lines or four parameter sigmoidal curves. N = 4 (Gq) or 3 (all other G proteins) independent experiments. **(H)** Illustration of NTSR1 G protein activation in TRUPATH assay following application of NT alone and in the presence of SR142948A or SBI-553. All data are presented as mean ± s.e.m. For curve parameters, see Supplementary Table 8. Supporting main text Fig. 2. Illustrations in **a**,**h** created using BioRender (Slosky, L. (2025) https://BioRender.com/8dgou51 and https://BioRender.com/4qtymyd).

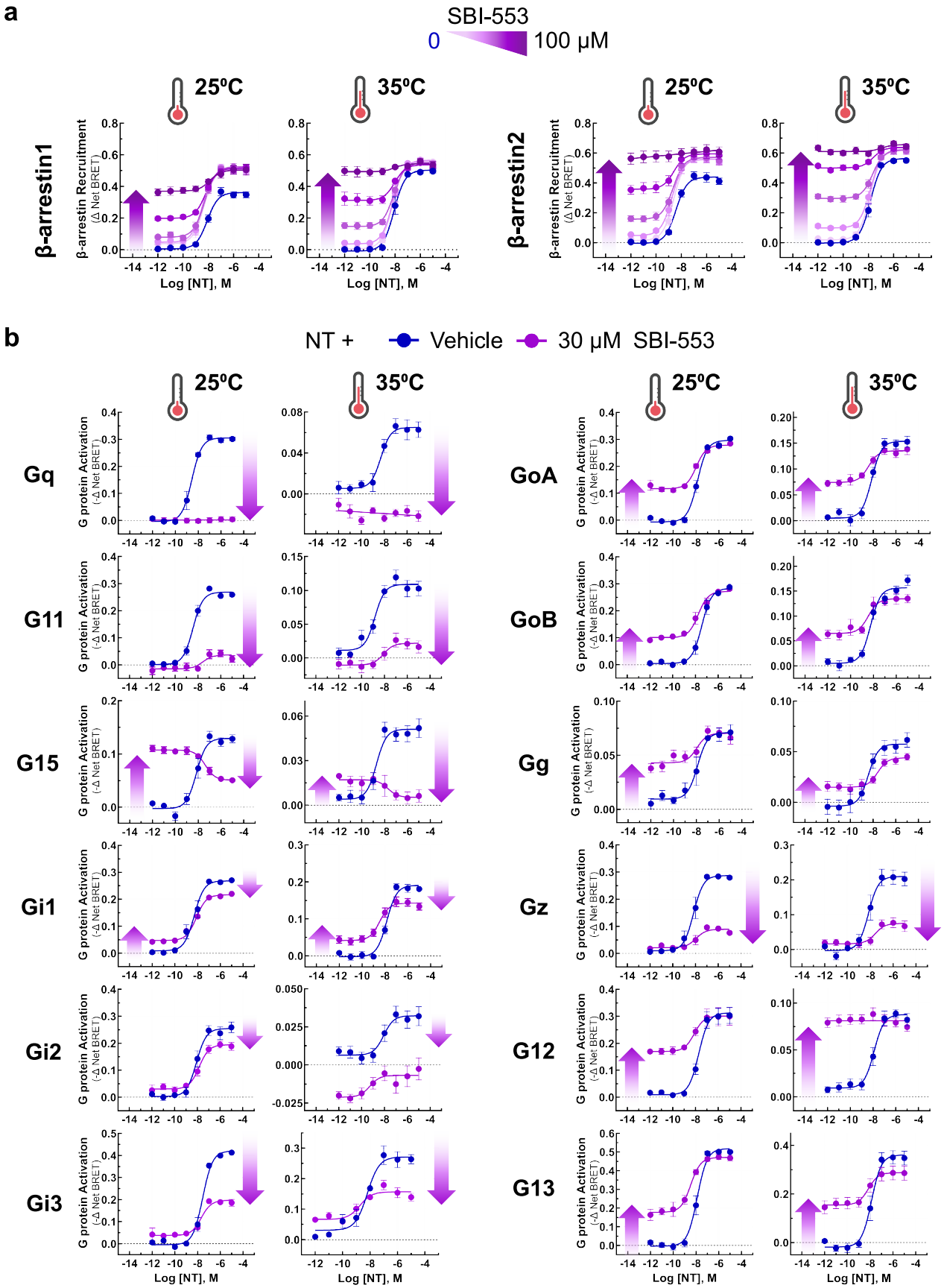

Extended Data Fig. 3 | See next page for caption.

Extended Data Fig. 3 | SBI-553 exerts consistent effects on NT-induced transducer activation at 25 °C and 35 °C. (A) SBI-553 exerts consistent effects on NT-induced β-arrestin recruitment at 25 °C and 35 °C. Cells were treated with NT in the absence and presence of SBI-553 (1, 3, 10, 30, 100 μM). SBI-553 stimulated β-arrestin recruitment to the NTSR1 and permitted NT-induced β-arrestin recruitment at both 25 °C and 35 °C. BRET values reflect maximal Δ net BRETs over a 35 min time course. n = 3 independent experiments. The 25 °C data here are presented in Extended Data Fig. 2f and are reproduced here to facilitate visual comparison. **(B)** SBI-553 exerts consistent effects on NT-induced G protein activation at 25 °C and 35 °C. Cells were treated with NT in the absence and presence of SBI-553 (30 μM). BRET values reflect maximal Δ net BRETs over a 35 min time course. SBI-553 exhibited transducer-specific agonism and antagonism at both 25 °C and 35 °C. The directionality and extent of SBI-553's transducer-specific bias was broadly similar in both conditions. The 25 °C data here are also presented as part of a larger CRC family in main text Fig. 2c and are reproduced here to facilitate visual comparison. Of note, TRUPATH assay efficiency is reduced at 35 °C for most but not all sensors. The optimal temperature for maximizing sensor dynamic range was room temperature. 35 °C was selected to balance assay efficacy with a desire to assess effects at physiological temperature and maintain consistency with prior work. Data represent the mean ± S.E.M. of at least 3 independent experiments, N = 3 (β-arrestin-1/2), 8 (Gq), 5 (G11), 6 (G15), 7 (Gi1), 10 (Gi2), 3 (Gi3), 8 (GoA), 6 (GoB), 6 (Gg), 5 (Gz), 7 (G12), 5 (G13). All data are presented as mean ± s.e.m. Supporting main text Fig. 2.

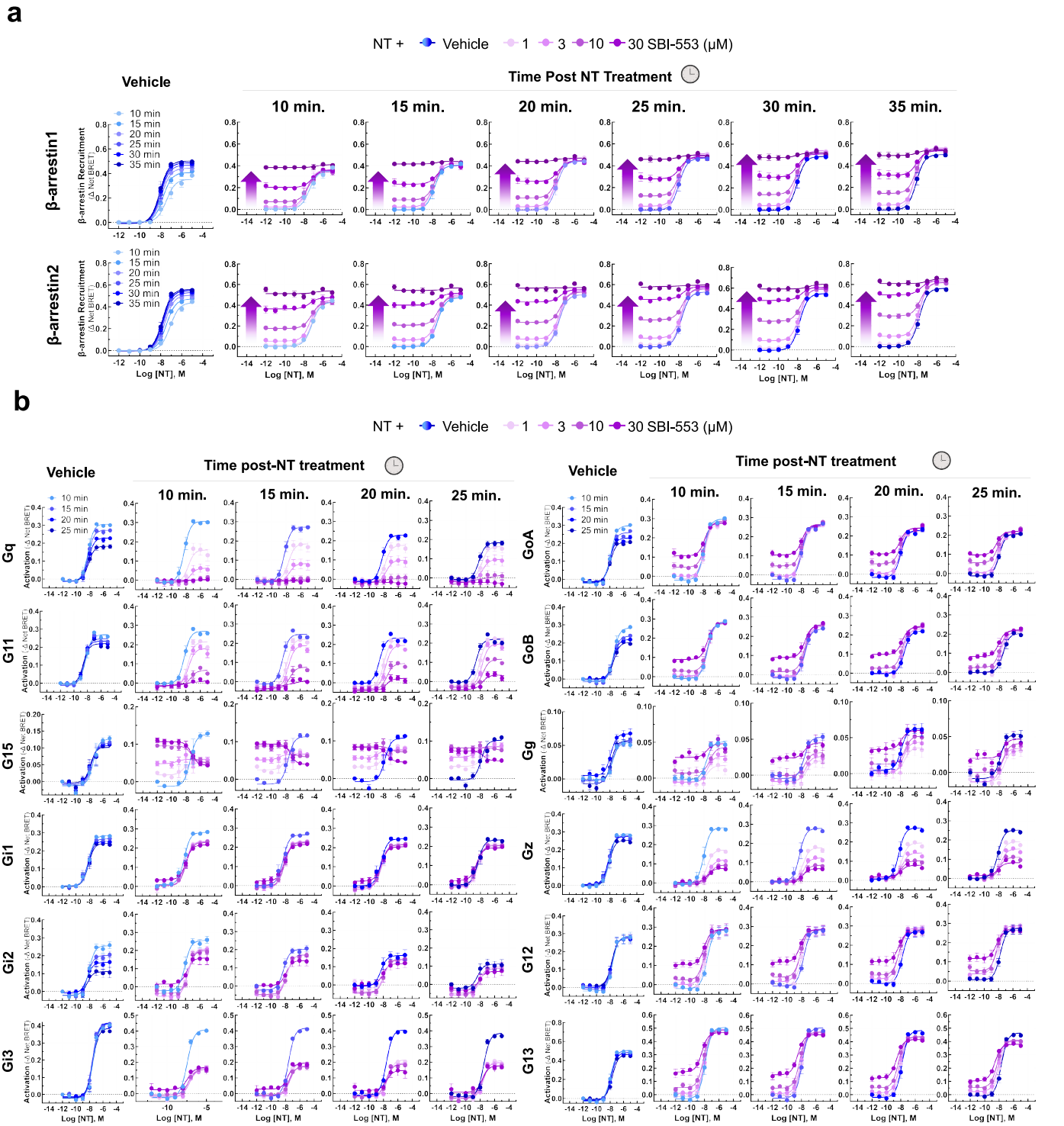

Extended Data Fig. 4 | Effect of SBI-553 on NT-induced transducer activation is stable over time. (A) β-arrestin recruitment. β-arrestin recruitment data presented elsewhere in this work reflect maximal Δ net BRETs between 10-35 min post NT treatment. To determine the effect of SBI-553 on NT-induced β-arrestin recruitment over time, we monitored recruitment between 10- and 35-min post treatment (35 °C). (Left) Effect of time on NT-induced β-arrestin recruitment to the NTSR1. β-arrestin recruitment in response to NT was greater at 35 min than 10 min. (Right) Effect of time on SBI-553 modulation of NT-induced β-arrestin recruitment. SBI-553 stimulated β-arrestin recruitment to the NTSR1 and permitted NT-induced β-arrestin recruitment at all time points. **(B)** G protein activation. TRUPATH G protein activation data presented elsewhere reflect maximal Δ net BRETs between 10–25 min post NT treatment. To determine the effect of SBI-553 on NT-induced G protein over time, we monitored activation between 10- and 25-min post treatment (25 °C). (Left columns) Effect of time on NT-induced G protein activation by TRUPATH. NTSR1 G protein activation following application of NT decreased with time for some G proteins (e.g., Gq, Gi2, GoA) and remained stable for others (e.g., Gi3, G12, G13). (Right columns) Effect of time on SBI-553 modulation of NT-induced NTSR1 G protein activation. SBI-553 exhibited transducer-specific agonism and antagonism over the entire time course. The directionality and extent of SBI-553's transducer-specific bias was broadly similar at all time points assessed. All data are derived from N = 3 independent experiments and are presented as mean ± s.e.m. Supporting main text Fig. 2.

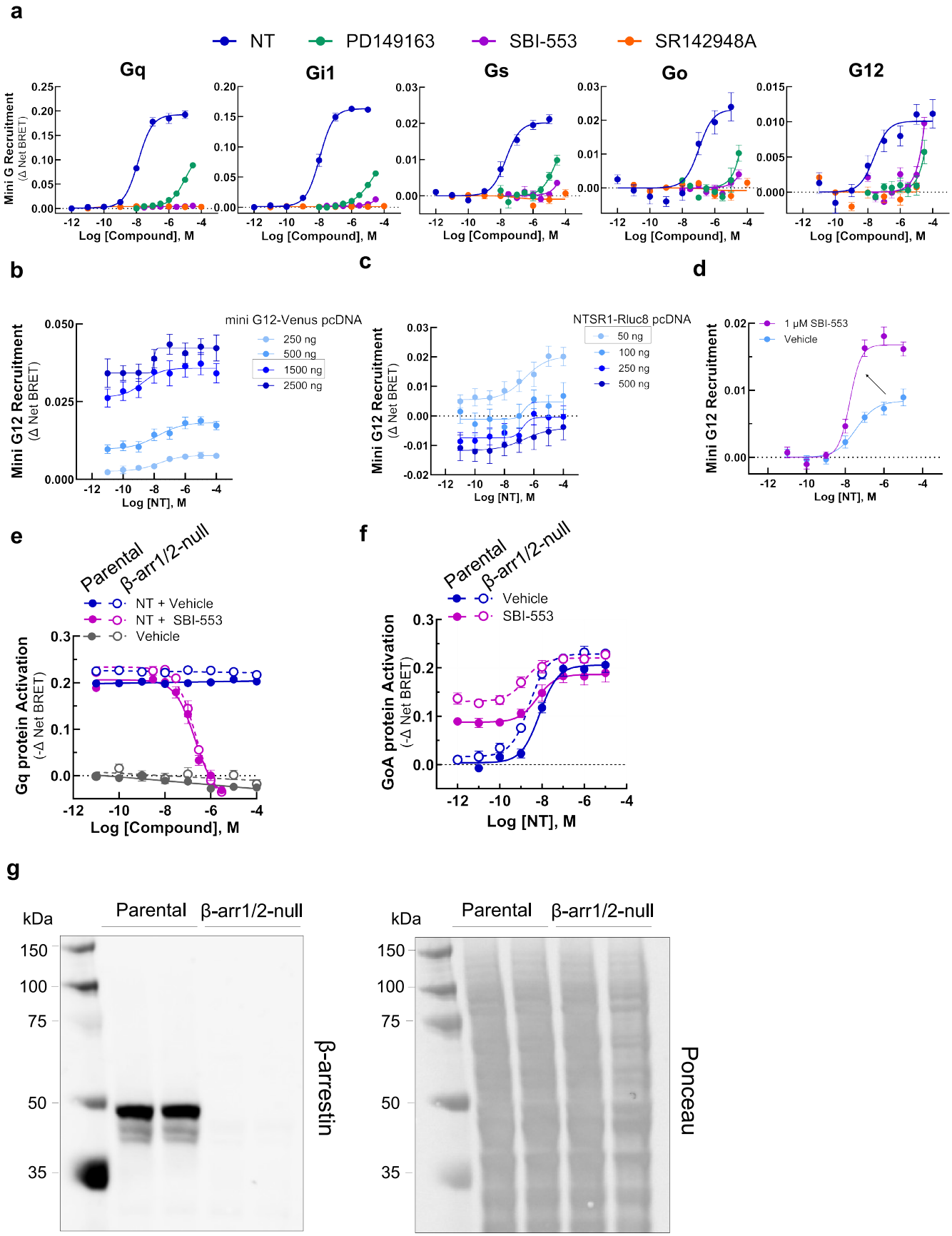

Extended Data Fig. 5 | See next page for caption.

Extended Data Fig. 5 | NT stimulates mini-G protein recruitment to the NTSR1, and SBI-553's effects on G protein activation are β-arrestin-1/2 independent. (A) Ligand-induced mini-G protein recruitment. Mini-G recruitment was assessed following NT, PD149163, SBI-553, and SR142948A treatment. Data are presented as mean ± s.e.m. N = 3 (Gq,Gi1,Gs,G12) or N = 4 (GoA) independent experiments. **(B-C)** Mini-G12 recruitment optimization. **(B)** BRET acceptor titration. NT-induced mini-G12 recruitment was assessed in HEK293T cells transiently expressing 100 ng NTSR1-Rluc8 and mini-G12-mVenus (250 ng, 500 ng, 1500 ng, or 2500 ng). N = 4 independent experiments. **(C)** BRET donor titration. NT-induced mini-G12 recruitment was assessed in HEK293T cells transiently expressing 1500 ng of mini-G12-mVenus and NTSR1-Rluc8 NTSR1 (50 ng, 100, ng, 250 ng, or 500 ng). N = 3 independent experiments. **(D)** SBI-553 enhances NT-induced mini-G12 recruitment. NT-induced Mini-G12 recruitment in the presence of SBI-553 (1 μM) or vehicle was assessed in HEK293T cells transiently expressing NTSR1-Rluc8 (50 ng) and mini-G12-mVenus (1500 ng). N = 3 independent experiments. **(E-G)** SBI-553 antagonism of Gq activation and agonism of GoA are independent of β-arrestin-1/2. **(E)** NT (100 nM)-induced Gq activation by TRUPATH was assessed following pretreatment with vehicle or SBI-553 in β-arrestin-1/2-null cells or their HEK293 parental line. SBI-553 was equally potent and effective in both cell lines. **(F)** GoA activation by TRUPATH was assessed following NT application with 30 μM SBI-553 or vehicle. SBI-553 agonized GoA in both β-arrestin-1/2-null and parental cells. N = 3 independent experiments. **(G)** Validation of β-arrestin-1/2-null cells by Western blot analysis. β-arrestin-1/2 deletion in null cells was confirmed by Western blot analysis. To ensure equal protein loading, membranes were stained with Ponceau S prior to antibody detection. A representative blot is shown with samples loaded in technical duplicates. For gel source data, see Supplementary Figure 1. Data are presented as mean ± s.e.m. Supporting main text Fig. 3.

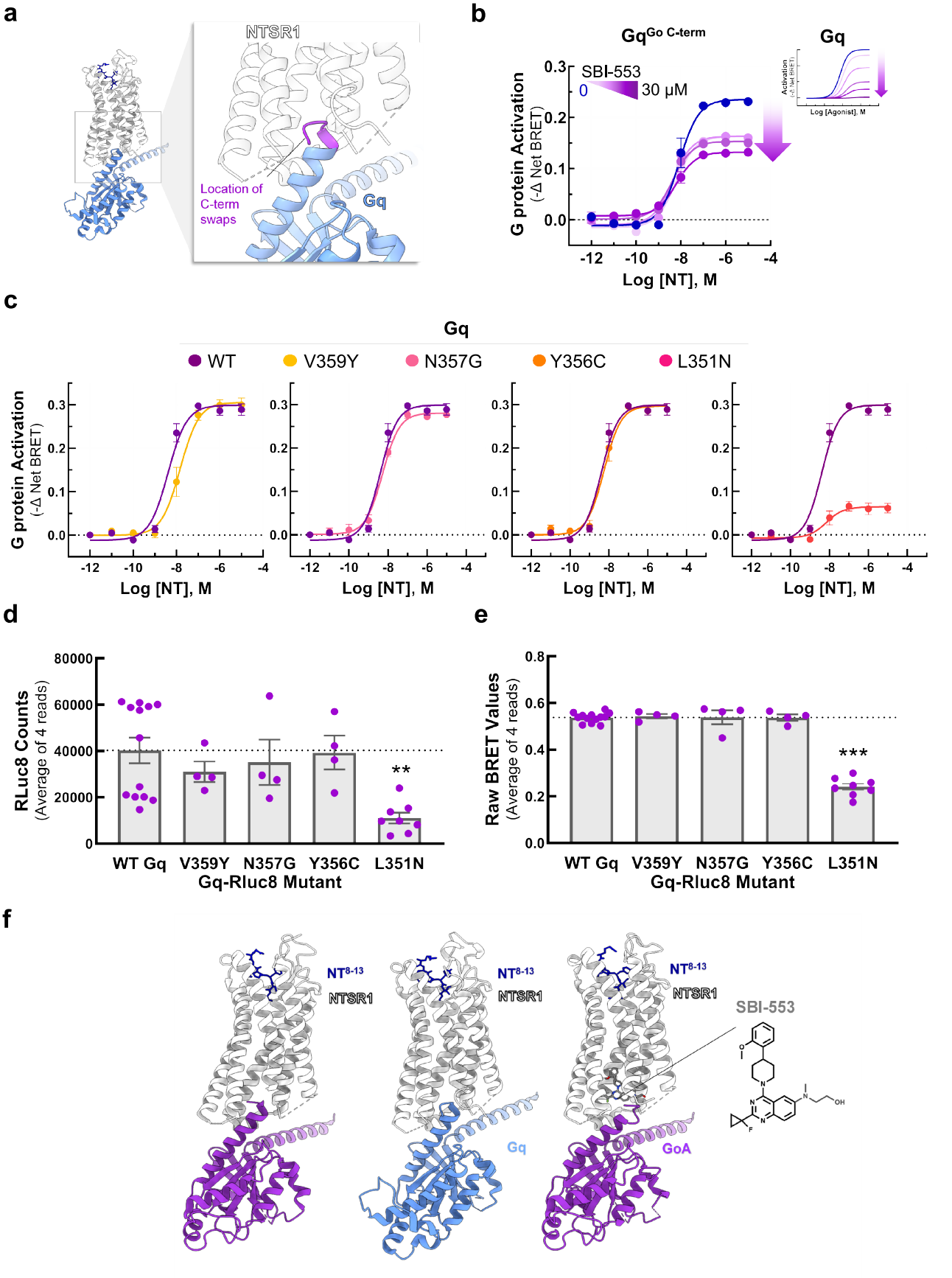

Extended Data Fig. 6 | See next page for caption.

Extended Data Fig. 6 | NT-induced activation and relative expression of G_q–Rluc8 mutants. (A) Location of the GoA/Gq 5 C-terminal amino acid residue swap. **(B)** Swapping Gq's 5 C-terminal amino acids for those of GoA reduces the antagonist efficacy of SBI-553. Inset, effect of SBI-553 on NT-induced activation of WT Gq for reference. N = 3 independent experiments. **(C)** NT-induced activation of full-length WT and mutant Gq TRUPATH constructs. **(D-E)** Relative expression of Gq-Rluc8 mutants was determined by total Rluc8 counts and level of heterotrimer formation was determined by basal BRET values. (**D**) Rluc8 emission and (**E**) basal BRET values from experiments presented in Fig. 4d. Rluc8 counts per plate were averaged over 4 reads. BRET values from unstimulated control wells were averaged over 4 reads. Dotted lines indicate mean values for WT Gq. Expression and heterodimer formation were intact in V359Y, N357G, and Y356C Gq mutants but reduced in the L351N mutant, relative to WT Gq. Data were analysed by one-way ANOVA followed by Tukey's multiple comparisons test F_{Rluc8} counts$(4, 28) = 4.533$, $p = 0.0060$. $^{**}p < 0.001$ L351N vs. WT Gq. $F_{Raw\ BRET\ values}(4, 28) = 126.1$, $p < 0.0001$. $^{***}p < 0.0001$ L351N vs. WT Gq. **(F)** Cryo-EM structures showing NTSR1 bound by the NT active fragment and G protein in the absence and presence of SBI-553. (Left) NTSR1, NT, mini-GoA (PDB 8FN1). (Middle) NTSR1, NT, mini-Gq (PDB 8FMZ). (Right) NTSR1, NT, SBI-553, mini-GoA (PDB 8FN0). All data are presented as mean ± s.e.m. For curve parameters, see Supplementary Table 9. Supporting main text Fig. 4.

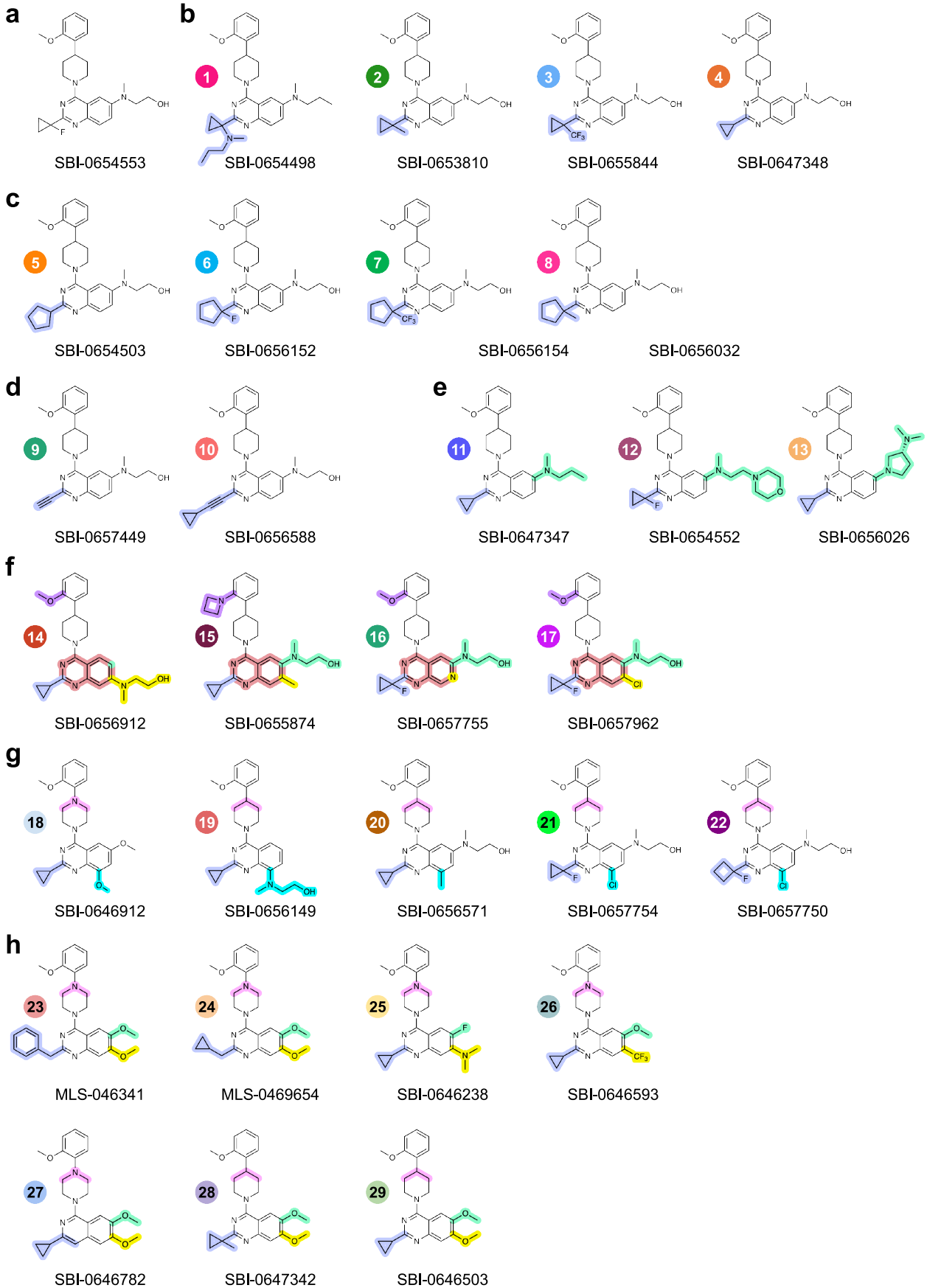

Extended Data Fig. 7 | See next page for caption.

Extended Data Fig. 7 | Structures of SBI-553 derivatives screened. Shaded atoms indicate structural changes at this position in the subgroup. **(A)** SBI-553 with selected quinazoline carbons numbered. **(B)** Changes in cyclopropane substituents (blue shading). **(C)** Replacing substituted cyclopentanes for cyclopropanes at the quinazoline 2-position (blue shading). **(D)** Alkyne substitution at the quinazoline 2-position (blue shading). **(E)** Changes to the quinazoline 6-position (green shading) with group of different rigidity, basicity, and polarity. **(F)** Changes in substitution at the quinazoline 7-position (yellow shading). **(G)** Changes to the quinazoline 8-position (purple shading). **(H)** Dimethoxy (early hit) compounds and related analogues. Supporting main text Fig. 5.

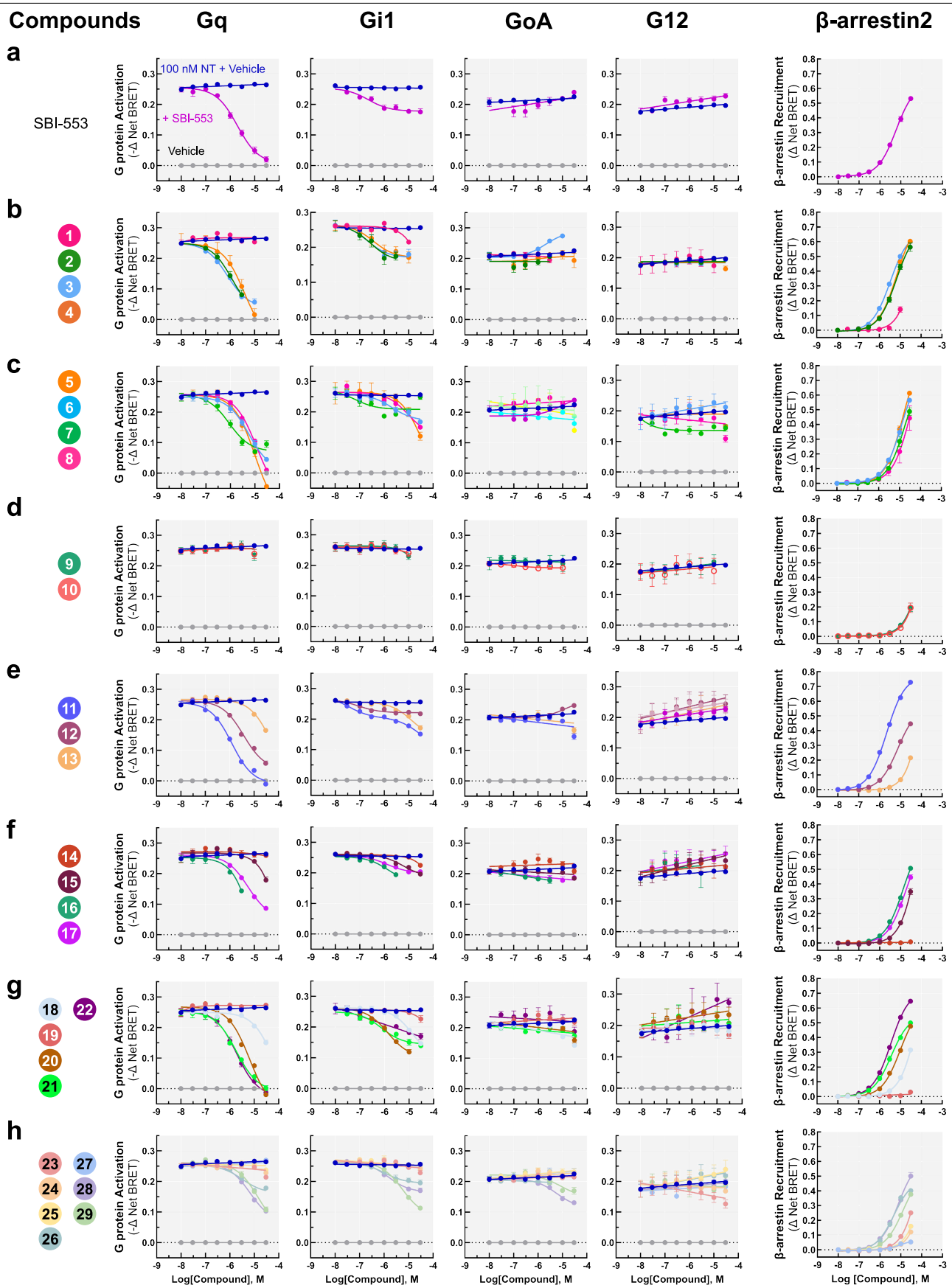

Extended Data Fig. 8 | See next page for caption.

Extended Data Fig. 8 | Screen of SBI-553 derivatives in assessments of G_q, G_{i1}, G_o and G_{12} antagonism and β-arrestin agonism. In HEK293T cells transiently expressing NTSR1, SBI-553, and 29 selected analogues (300 nM - 30 μM) were assessed for their ability to antagonize 100 nM NT-induced G protein activation by TRUPATH and stimulate β-arrestin-2 recruitment independently by BRET. Compound screen IDs (1–29) are provided at right. **A**–**H** contain data for compounds with structures presented in corresponding Extended Data Fig. 7a–h. Data were fitted to lines or four parameter sigmoidal curves. Some compounds selected for follow-up analyses produced non-NTSR1 mediated effects on G protein sensor activity. Concentrations producing these effects have been removed. Vehicle, 3% β-HB-cyclodextrin, <0.25% DMSO in HBSS. All data are presented as mean ± s.e.m. N = 3 independent experiments. For curve parameters, see Supplementary Table 10. Supporting main text Fig. 5.

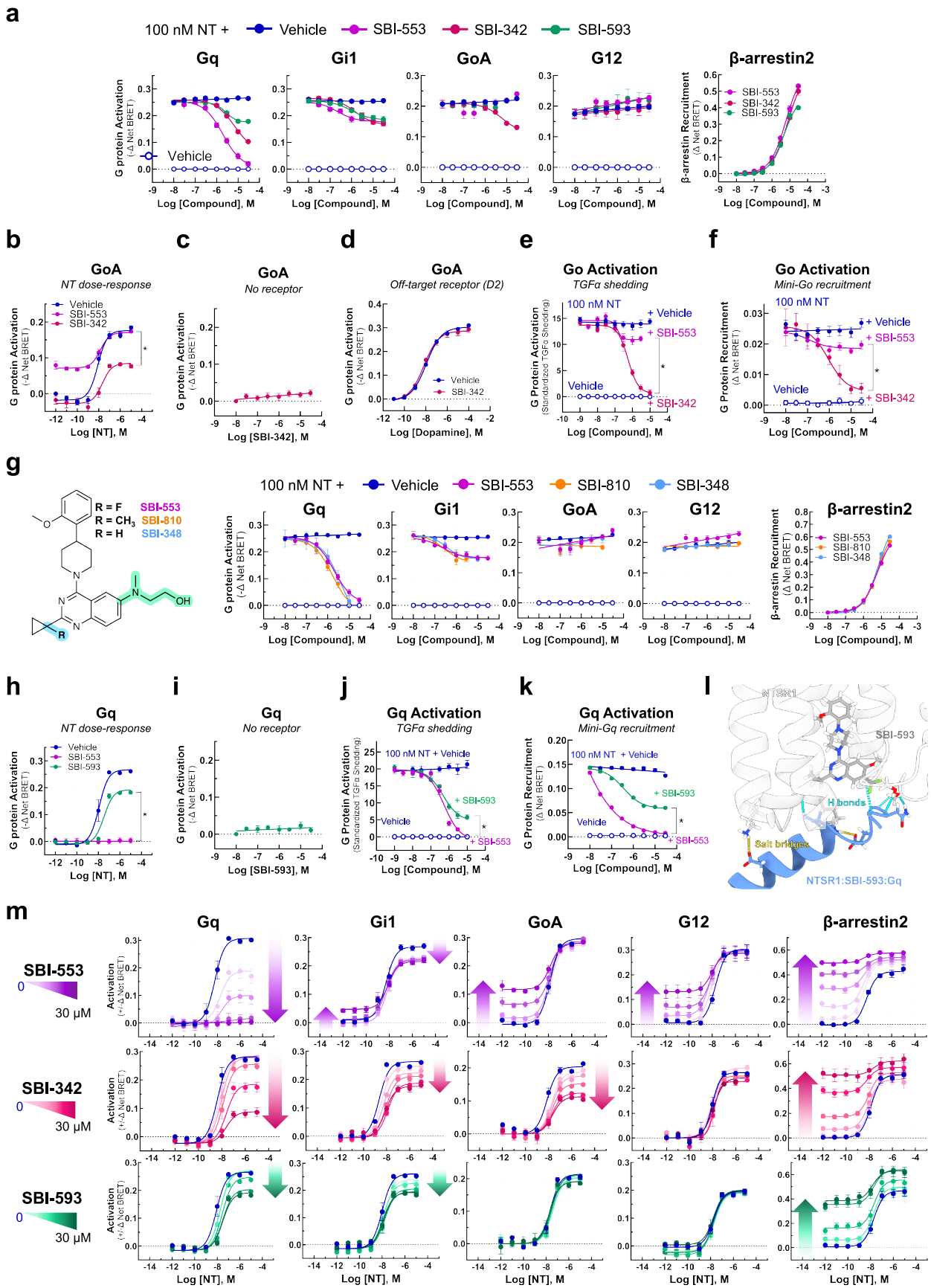

Extended Data Fig. 9 | See next page for caption.

Extended Data Fig. 9 | Validation of SBI-553 analogues with distinct transducer selectivity profiles. (A) SBI-553, SBI-342, and SBI-593 antagonism of NT-induced Gq, Gi1, GoA, and G12 activation by TRUPATH and agonism of β-arrestin-2 by BRET. **(B–F)** Analogue SBI-342 exhibits Go antagonism, not agonism. **(B)** Effect of 30 μM SBI-553 vs SBI-342 across the NT GoA CRC. **(C)** Assessment of SBI-342 on GoA TRUPATH activation sensor activity in HEK293T cells not expressing NTSR1. **(D)** Assessment of SBI-342 (30 μM) on GoA activation stimulated by the Gi/o-coupled dopamine receptor D2. **(E)** SBI-553 and SBI-342 antagonism of NT-induced Go activation in the AP-TGFα shedding assay. **(F)** SBI-553 and SBI-342 antagonism of NT-induced mini-GoA recruitment to the NTSR1. **(G)** Neither substitution nor removal of SBI-553's fluorine affects G protein selectivity. (Left) Structural comparison of SBI-553, SBI-810, and SBI-348. (Right) SBI-553, SBI-342, and SBI-593 antagonism of NT-induced Gq, Gi1, GoA, and G12 activation by TRUPATH and agonism of β-arrestin-2 by BRET. The 30 μM SBI-810 and SBI-348 concentrations produced nonspecific effects and were excluded. **(H–L)** Analogue SBI-593 exhibits partial rather than full Gq antagonism. **(H)** Effect of 30 μM SBI-553 vs SBI-593 across the NT Gq CRC. **(I)** Assessment of SBI-593 on Gq TRUPATH activation sensor activity in HEK293T cells not expressing NTSR1. **(J)** SBI-553 and SBI-593 antagonism of NT-induced Gq activation in the AP-TGFα shedding assay. **(K)** SBI-553 and SBI-593 antagonism of NT-induced mini-GoA recruitment to the NTSR1. **(L)** Interactions stabilizing the SBI-593-induced new Gq position are shown. **(M)** CRC curve families for NT in the absence and presence of −553, −342 and, −593. For all panels, all data from N = 3 independent experiments are presented as mean ± s.e.m. *indicates non-overlapping 95% confidence intervals for indicated curve bottoms. For curve parameters, see Supplementary Table 11. Supporting main text Fig. 5.

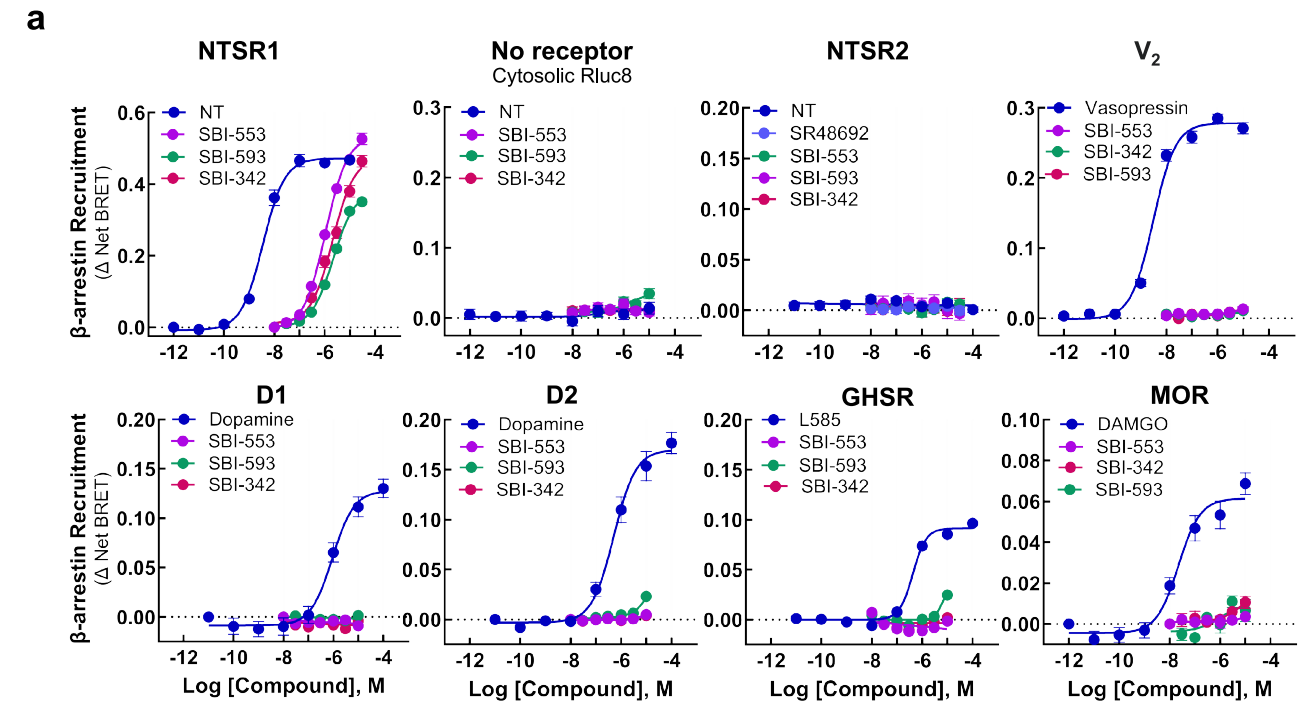

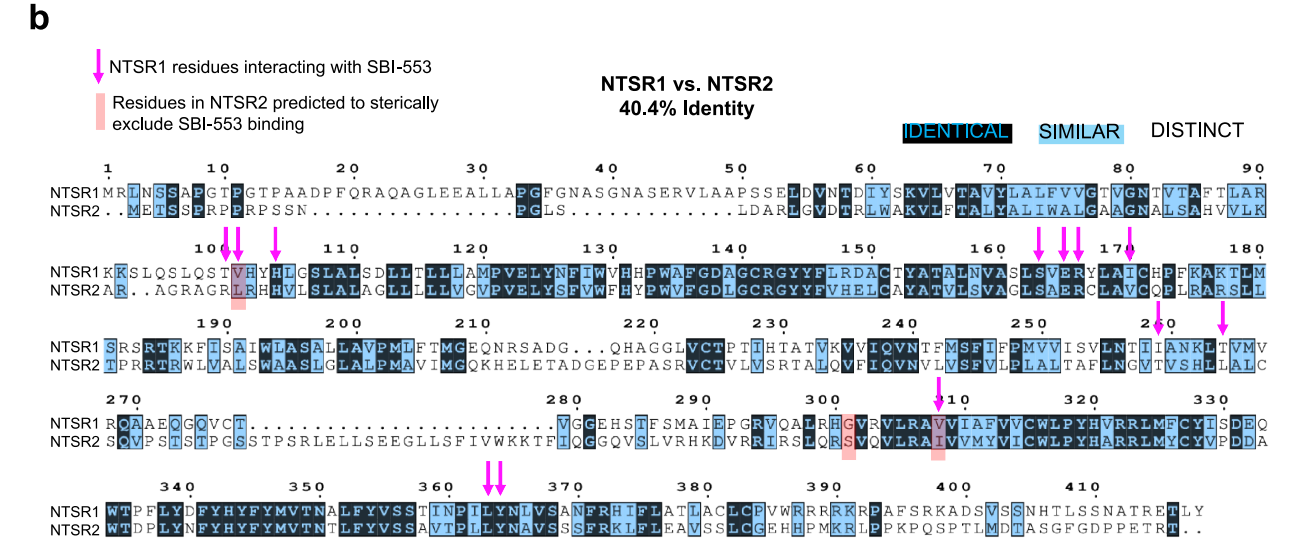

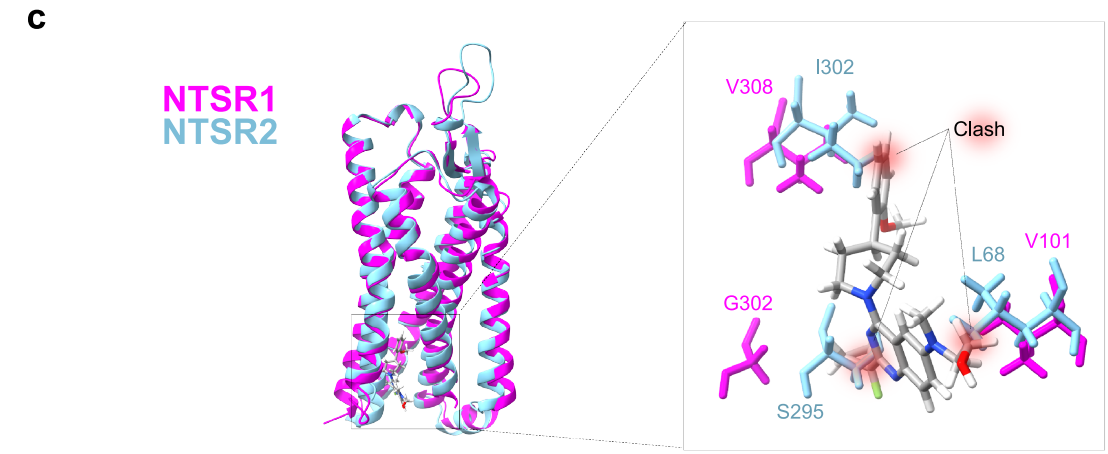

Extended Data Fig. 10 | See next page for caption.

Extended Data Fig. 10 | SBI compound selectivity assessment. (A) Recruitment of Venus-tagged human β-arrestin-2 to multiple *Renilla* luciferase-tagged human GPCRs was assessed in HEK293T cells by BRET. Selected receptors: NTSR1 (positive control), no receptor, cytosolic Rluc8 (negative control), NTSR2, vasopressin V2 receptor (V_2), dopamine D1 receptor (D1R), dopamine D2 receptor (D2R), ghrelin receptor (GHSR), and mu-opioid receptor (MOR). All receptors except NTSR2 responded to selected agonist control compounds. Only NTSR1 exhibited concentration-dependent β-arrestin-2 recruitment that could be fit to a sigmoidal curve in response to SBI-553, SBI-593, and SBI-342. All data are presented as mean ± s.e.m. N = 3 independent experiments. **(B)** NTSR1 and NTSR2 sequence alignments. To better understand why this compound series would not bind NTSR2, we aligned the human NTSR1 and NTSR2 amino acid sequences obtained from NCBI. Residues in NTSR1 identified as interacting with SBI-553 are indicated by pink arrows. Note 5 of 12 positions highlighted by these arrows are not identical. **(C)** NTSR1 and NTSR2 structure alignments. A predicted AlphaFold structure of human NTSR2 was generated and aligned with an SBI-553-bound NTSR1 cryo-EM structure (PDB 8FN0). In addition to missing key interacting residues, the shape of the NTSR2 pocket appears to sterically exclude compounds with the SBI-553 scaffold. Supporting main text Fig. 5.

a

	Human	Macaque	Dog	Mini Pig	Rat	Mouse
Human (*Homo sapiens*)	x					
Macaque (*Macaca mulatta*)	98.6	x				
Dog (*Canis familiaris*)	85.3	85	x			
Mini Pig (*Sus scrofa*)	84	83.5	85.3	x		
Rat (*Rattus norvegicus*)	83.5	84	81.7	79.2	x	
Mouse (*Mus musculus*)	84.5	84.7	82.2	79.5	93	x
Human NTSR2	40.4	40.4	40.5	42.7	40	40.1

b

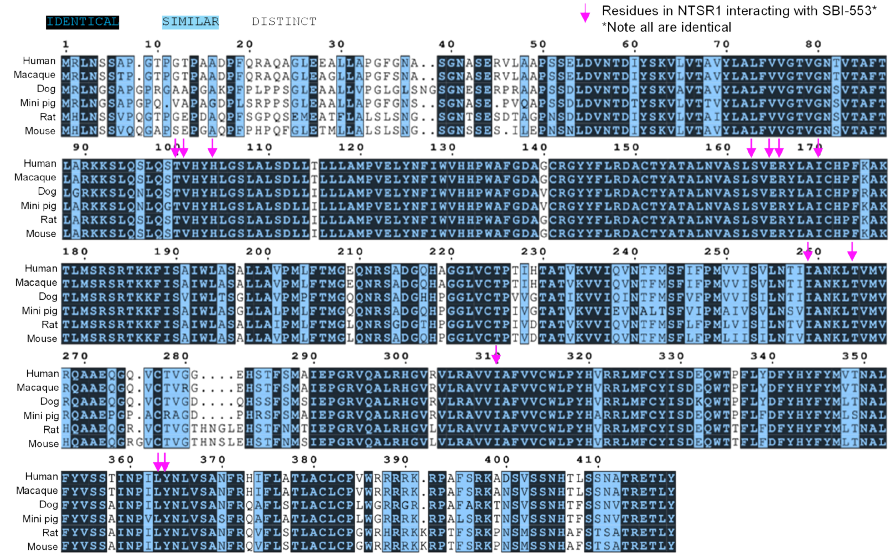

d

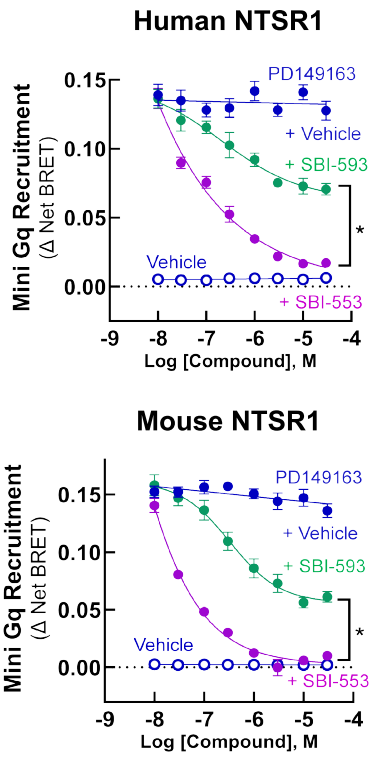

c

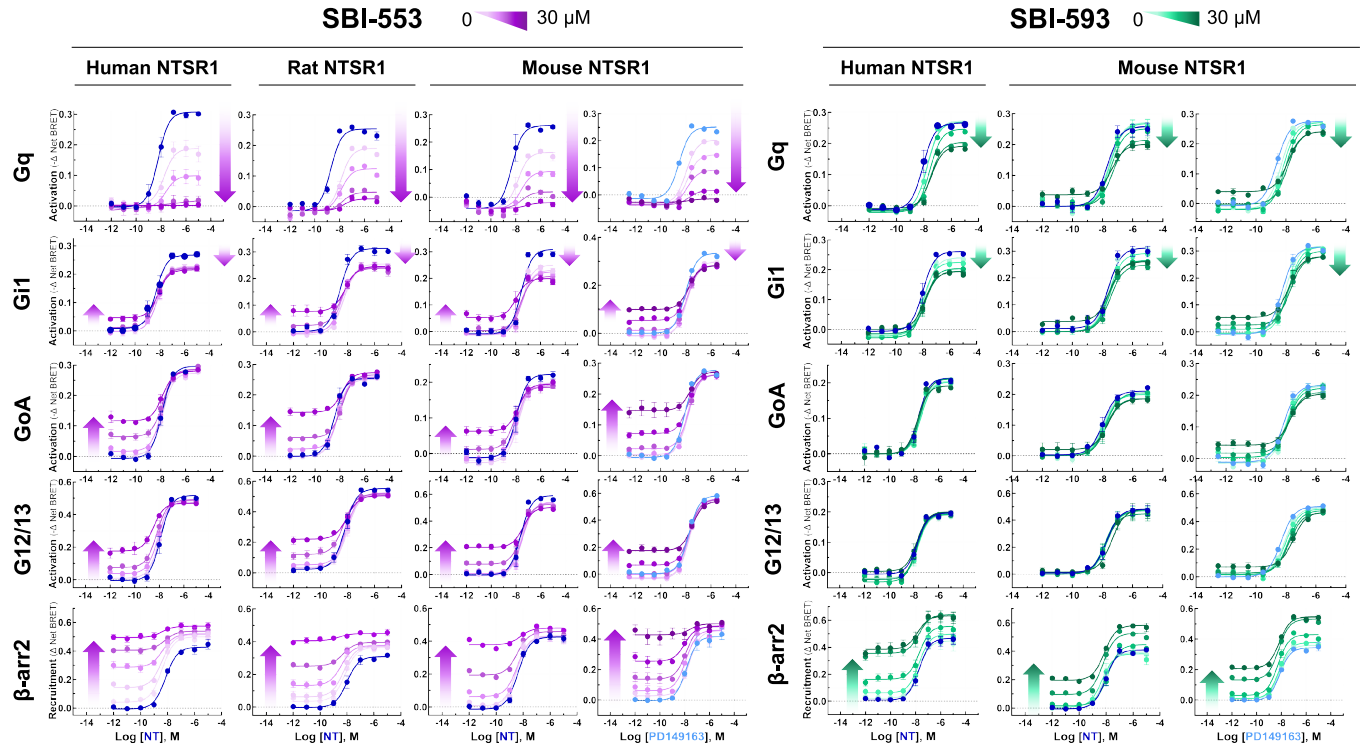

Extended Data Fig. 11 | See next page for caption.

Extended Data Fig. 11 | The SBI-553-binding pocket and SBI compound signalling signatures are conserved across NTSR1 species. (A) NTSR1 per cent amino acid identity by species. Per cent (%) sequence identity of NTSR1 from commonly used pre-clinical mammalian species. NTSR2 is included for context. Reference sequences that were obtained from NCBI. **(B)** NTSR1 sequence alignments by species. Alignments of the NTSR1 primary sequence by species. Positions with identical residues are indicated by a black background colour. Residues in the human and rodent NTSR1 identified as interacting with SBI-553 and forming the SBI-553 binding pocket are indicated by pink arrows. Note that all positions with pink arrows are identical. Sequences were aligned using the BLOSUM62 matrix in ClustalW. Similarities were calculated using the Expasy server. **(C)** SBI compound signalling profiles at the human and rodent NTSR1. Activation of representative G protein family members and β-arrestin was assessed in HEK293T cells expressing human, rat, or mouse NTSR1 following application of NT or PD149163 in the absence and presence of SBI-553 (0.3, 1, 3, 10, 30 μM). The directionality and extent of SBI-553's transducer-specific bias was broadly similar at all NTSR1s evaluated and in the presence of both orthosteric agonists. **(D)** SBI-593 partially antagonizes PD149163-induced Gq mini-Gq recruitment to both the human and mouse NTSR1. In HEK293T cells transiently expressing NTSR1, the PD149163-induced association between NTSR1 and mini-Gq was assessed by BRET. Effect of SBI-553 and SBI-593 on Gq association with the (top) human and (bottom) mouse NTSR1. *indicates non-overlapping 95% confidence intervals for indicated curve bottoms. Data from N = 3 independent experiments are presented as mean ± s.e.m. For selected panels (Gi1, SBI-553 + NT, human; GoA, SBI-553 + NT, mus; β-arrestin-2, SBI-553 + NT, human) N = 4. Supporting main text Fig. 6.

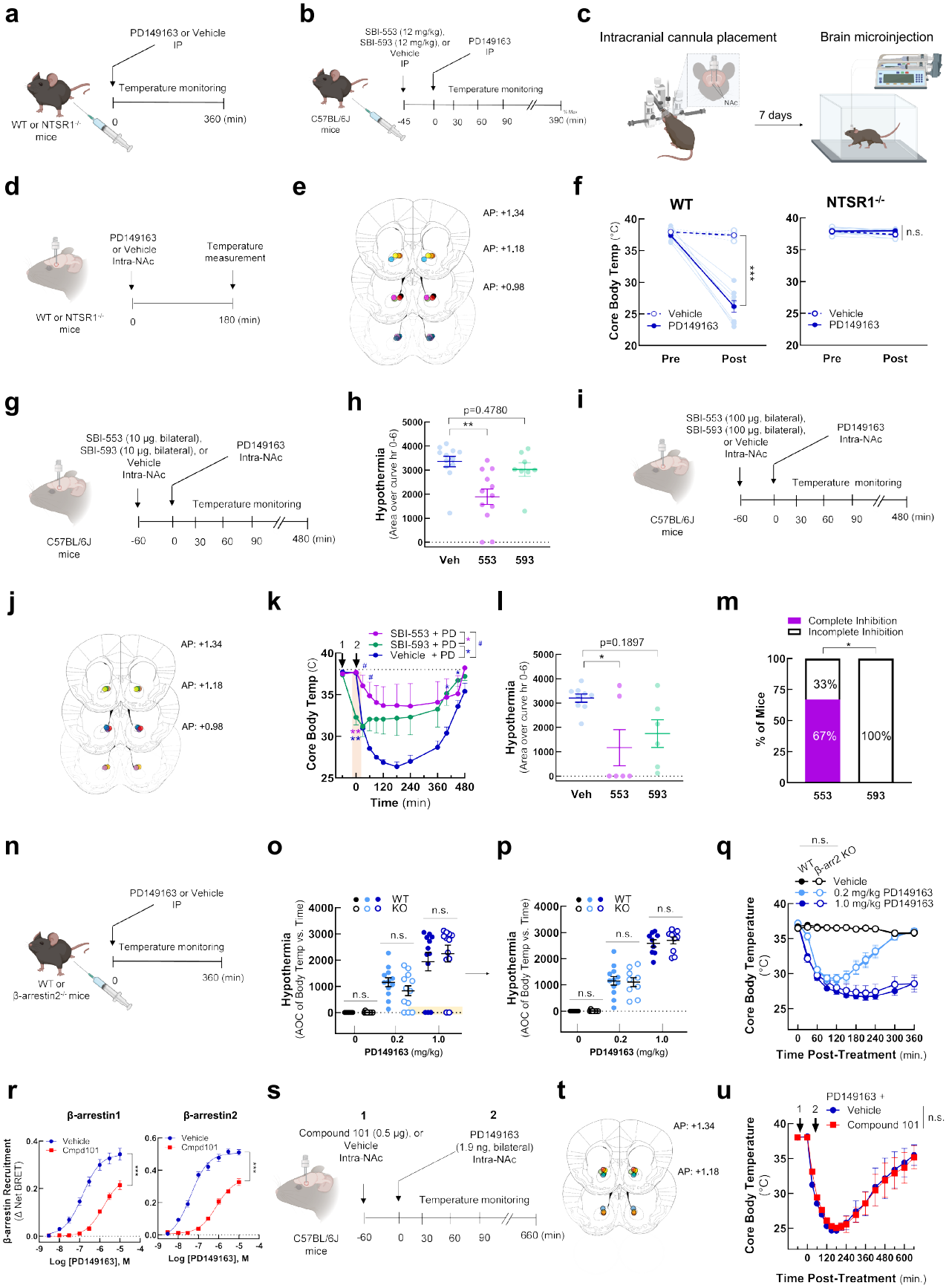

Extended Data Fig. 12 | See next page for caption.

Extended Data Fig. 12 | PD149163-induced hypothermia and its blockade by NTSR1 BAMs. (A) Experimental timeline for Fig. 6a. **(B)** Experimental timeline for Fig. 6c. **(C)** Overview of bilateral intracranial cannula placement targeting the NAc core in mice. **(D–F)** Intra-NAc PD149163 induces NTSR1-dependent hypothermia in mice. **(D)** Experimental timeline. **(E)** Ink-verified cannula placements for mice. Numbers denote mm in front of bregma. AP, anterior–posterior. **(F)** Effect of intra-NAc microinjection of PD149163 (93 ng, bilateral) in WT and *Ntsr1*$^{-/-}$ mice. Two-way, repeated measures ANOVA,***p < 0.0001. N (mice/group)= 8 WT PD149163, 6 *Ntsr1*$^{-/-}$ PD149163, 6 WT vehicle, 6 *Ntsr1*$^{-/-}$ vehicle. **(G,H)** 10 µg SBI-553 but not SBI-593 intra-NAc attenuates PD149163-induced hypothermia. **(G)** Experimental timeline for Fig. 6e. **(H)** Area over the curve for data in Fig. 6e. Baseline set at 37 °C. Kruskal-Wallis test followed by Dunn's multiple comparisons, **p < 0.001. N (mice/group) = 12 vehicle, 12 SBI-553, 8 SBI-593. **(I-M)** 100 µg intra-NAc SBI-593 administration partially attenuates PD149163-induced hypothermia. **(I)** Experimental timeline. **(J)** Ink-verified cannula placements. **(K)** Effect of intra-NAc SBI-553 (100 µg, bilateral) and SBI-593 (100 µg, bilateral) on PD149163 (9.3 ng, bilateral, intra-NAc)-induced hypothermia. Mixed-model ANOVA followed by Tukey's multiple comparisons test, **,##p < 0.01, *#p < 0.05. N (mice/group) = 6 SBI-553, 6 SBI-593, 9 vehicle. **(L)** Area over the curve for data in panel **k**. Baseline set at 37 °C. Kruskal-Wallis test followed by Dunn's multiple comparisons,*p < 0.05. **(M)** Proportion of mice exhibiting complete vs. incomplete blockade of PD149163-induced hypothermia by treatment group. Two-sided chi-square, *p < 0.01. **(N–Q)** The extent and duration of PD149163-induced hypothermia is unchanged in *Arrb2*$^{-/-}$ mice. (**N**) Experimental timeline. **(O)** Total hypothermia over the 6-hour time course, quantified as the area over the body temperature vs. time curve. Baseline was set at 37 °C. Two-way ANOVA, p = 0.98. N (mice/genotype/treatment group) = 12, except for the *Arrb2*$^{-/-}$ vehicle group for which N = 10. 5 *Arrb2*$^{-/-}$ and 3 WT mice in the PD149163 treatment groups (highlighted in yellow) were identified as outliers (ROUT method, Q = 2%). To determine whether these outlying values masked a genotype effect, data were excluded and the analysis re-run. **(P)** Exclusion of PD149163 non-responders did not reveal an effect of β-arrestin-2 deletion on PD149163-induced hypothermia. Two-way ANOVA, p = 0.82. **(Q)** Time course of PD149163-induced hypothermia in *Arrb2*$^{-/-}$ and WT mice. Two-way, repeated measures ANOVA, p = 0.66. N = 12 (WT, Veh), 12 (WT, 0.2 mg/kg), 9 (WT, 1.0 mg/kg), 10 (*Arrb2*$^{-/-}$, Veh), 9 (*Arrb2*$^{-/-}$, 0.2 mg/kg), 10 (*Arrb2*$^{-/-}$, 1.0 mg/kg). (**R–U**) GPCR kinase (GRK) 2/3 inhibition attenuates PD149163-induced β-arrestin recruitment but not hypothermia. **(R)** Effect of GRK2/3 inhibitor Compound 101 (Cmpd101) on SBI-553-induced β-arrestin-1/2 recruitment. Extra sum of squares F test, *p < 0.01. N = 4 independent experiments. (**S**) Experimental timeline. (**T**) Ink-verified cannula placements. (**U**) Effect of intra-NAc Cmpd101 (0.5 µg, bilateral) on PD149163 (1.9 ng, bilateral, intra-NAc)-induced hypothermia in C57BL/6 J mice. Two-way repeated measures ANOVA, p = 0.99. N (mice/group) = 4. All data are presented as mean ± s.e.m. For curve parameters and comparison details, see Supplementary Table 12. Supporting main text Fig. 6. Brain illustrations in **e**,**j**,**t** adapted with permission from ref. 53, Elsevier. Illustrations in **a**–**d**,**g**,**i**,**n**,**s** created using BioRender (Slosky, L. (2025) https://BioRender.com/tcmavuc, https://BioRender.com/h9zsd3v and https://BioRender.com/fb62wq2).

nature portfolio

Corresponding author(s): Lauren M. Slosky

Last updated by author(s): Aug 22, 2025

Reporting Summary

Nature Portfolio wishes to improve the reproducibility of the work that we publish. This form provides structure for consistency and transparency in reporting. For further information on Nature Portfolio policies, see our Editorial Policies and the Editorial Policy Checklist.

Statistics

For all statistical analyses, confirm that the following items are present in the figure legend, table legend, main text, or Methods section.

n/a	Confirmed
☐	☒ The exact sample size (*n*) for each experimental group/condition, given as a discrete number and unit of measurement
☐	☒ A statement on whether measurements were taken from distinct samples or whether the same sample was measured repeatedly
☐	☒ The statistical test(s) used AND whether they are one- or two-sided *Only common tests should be described solely by name; describe more complex techniques in the Methods section.*
☒	☐ A description of all covariates tested
☐	☒ A description of any assumptions or corrections, such as tests of normality and adjustment for multiple comparisons
☐	☒ A full description of the statistical parameters including central tendency (e.g. means) or other basic estimates (e.g. regression coefficient) AND variation (e.g. standard deviation) or associated estimates of uncertainty (e.g. confidence intervals)
☐	☒ For null hypothesis testing, the test statistic (e.g. *F*, *t*, *r*) with confidence intervals, effect sizes, degrees of freedom and *P* value noted *Give P values as exact values whenever suitable.*
☒	☐ For Bayesian analysis, information on the choice of priors and Markov chain Monte Carlo settings
☒	☐ For hierarchical and complex designs, identification of the appropriate level for tests and full reporting of outcomes
☒	☐ Estimates of effect sizes (e.g. Cohen's *d*, Pearson's *r*), indicating how they were calculated

Our web collection on statistics for biologists contains articles on many of the points above.

Software and code

Policy information about availability of computer code

Data collection	Images of NTSR1 and G protein structures were created in ChimeraX (v1.6, UCSF). Homology models of each G protein were built with MOE (v2022.02, Chemical Computing Group, Montreal, CA) with the conformation of each mutated side chain optimized individually using the Amber 10:EHT force field built into MOE. The free energy required to dissociate the individual NT-NTSR1-SBI-553-'open' position G protein complexes created by homology modeling was estimated using 'Protein interfaces, surfaces and assemblies' service PISA at the European Bioinformatics Institute (http://www.ebi.ac.uk/pdbe/prot_int/pistart.html). Minimization of the protein complexes containing SBI-342 and SBI-593 utilized the OPLS4 force field in Maestro (v14.1.138 Schrödinger, Inc., NY, NY). Molecular dynamics simulations with Gq and SBI-593 were conducted with Desmond using the Schrödinger suite (v13.7.125 and v14.3.129). Illustrations were created with BioRender.
Data analysis	Data were analyzed and plotted using the software GraphPad Prism version 10.1.2.

For manuscripts utilizing custom algorithms or software that are central to the research but not yet described in published literature, software must be made available to editors and reviewers. We strongly encourage code deposition in a community repository (e.g. GitHub). See the Nature Portfolio guidelines for submitting code & software for further information.

Data

Policy information about availability of data

All manuscripts must include a data availability statement. This statement should provide the following information, where applicable:

- Accession codes, unique identifiers, or web links for publicly available datasets
- A description of any restrictions on data availability
- For clinical datasets or third party data, please ensure that the statement adheres to our policy

The data that support the findings of this study are available in the Supplemental Information, provided as source data, and deposited in the Harvard Dataverse under https://doi.org/10.7910/DVN/J10DSJ. Additional information and materials are available from the corresponding author upon request.

Research involving human participants, their data, or biological material

Policy information about studies with human participants or human data. See also policy information about sex, gender (identity/presentation), and sexual orientation and race, ethnicity and racism.

Reporting on sex and gender	NA
Reporting on race, ethnicity, or other socially relevant groupings	NA
Population characteristics	NA
Recruitment	NA
Ethics oversight	NA

Note that full information on the approval of the study protocol must also be provided in the manuscript.

Field-specific reporting

Please select the one below that is the best fit for your research. If you are not sure, read the appropriate sections before making your selection.

☒ Life sciences ☐ Behavioural & social sciences ☐ Ecological, evolutionary & environmental sciences

For a reference copy of the document with all sections, see nature.com/documents/nr-reporting-summary-flat.pdf

Life sciences study design

All studies must disclose on these points even when the disclosure is negative.

Sample size	Data from biochemical assays are presented as the average +/- SEM of at least three biological replicates (N), which are the minimum required for reproducibility and statistical validity, run on different experimental days, with cells from different transient transfections, and exposed to compound dilution series prepared separately. When parameter estimates were poorly constrained (wide confidence intervals), we performed additional replicates to strengthen the fit and improve reliability. The number of biological replicates for each study are provided in Supplemental Tables 1-6. A minimum of two technical replicates were included within each biological replicate. For PD149163-induced hypothermia studies, group numbers (N) are based on a power analysis (0.8) of preliminary data examining the effects of SBI-553 and C57BL/6L mice, using the effect size of the 12 mg/kg SBI-553 dose and the 0.2 mg/kg PD149163 dose. The number of mice in each individual experiment is provided in Supplemental Tables 1-6. For these between-subject assessments, mice were age- and sex-matched and randomly assigned to treatment groups. Because behavioral changes are sensitive to litter effects and environmental variables, we exclusively generated study KO and WT animals by HT X HT breeding, allowing littermate WT mice to serve as controls. All experiments will be performed with both male and female mice.
Data exclusions	Data from assay plates in which 1) a technical error on the part of the experimenter was identified or 2) a failure of either the positive or negative control was identified were excluded from the analysis. Exclusion criteria were pre-established.
Replication	Reproducibility of experimental findings was ensured through replication in multiple biological replicates in independent experiments. All attempts at replication were successful. All experiments will included positive (e.g., NT) and negative (e.g., SR142948A) controls, at least 2 technical replicates, and at least 3 biological replicates. Vehicle controls and assessments in HEK293 cells not expressing NTSR1 were included to rule out diluant and non-specific confounds. Assessments in genetically modified and cognate parental lines were in parallel, on the same assay plate.
Randomization	Mice were age- and sex-matched and randomly assigned to experimental groups. For biochemical assays potential sources of bias were controlled through parallel processing and replication; therefore, randomization was not required. All experiments included positive and negative controls, at least 2 technical replicates, and at least 3 biological replicates. Vehicle controls and assessments in HEK293 cells not

expressing NTSR1 were included to rule out dilutant and non-specific confounds. Assessments in genetically modified and cognate parental lines were run in parallel, on the same assay plate.

Blinding

Investigators were not blinded to experimental conditions. For biochemical studies, blinding was unnecessary as the experimental outcomes were derived from automated, ratiometric measurements rather than observer-dependent assessments. For animal studies, data acquisition was likewise quantitative in nature and did not require experimenter interpretation.

Reporting for specific materials, systems and methods

We require information from authors about some types of materials, experimental systems and methods used in many studies. Here, indicate whether each material, system or method listed is relevant to your study. If you are not sure if a list item applies to your research, read the appropriate section before selecting a response.

Materials & experimental systems

n/a	Involved in the study
☐	☒ Antibodies
☐	☒ Eukaryotic cell lines
☒	☐ Palaeontology and archaeology
☐	☒ Animals and other organisms
☒	☐ Clinical data
☒	☐ Dual use research of concern
☒	☐ Plants

Methods

n/a	Involved in the study
☒	☐ ChIP-seq
☒	☐ Flow cytometry
☒	☐ MRI-based neuroimaging

Antibodies

Antibodies used

Rabbit anti-β-Arrestin1/2 (Cell Signaling Technology, product #4674)
Alexa Fluor® goat anti-rabbit 680 (Invitrogen, Carlsbad, CA, #A-21109, RRID:AB_2535758)

Validation

Antibodies are commercially available and have been validated by vendors.

Eukaryotic cell lines

Policy information about cell lines and Sex and Gender in Research

Cell line source(s)

HEK293T/17 (Cat# CRL-11268, RRID:CVCL_1926) cells were obtained from the American Type Culture Collection (ATCC, Manassas, VA). G protein-deficient HEK293 cells (ΔGNAS, GNAL, GNAQ, GNA11, GNA12, and GNA13 HEK293 - Clone 38) and β-arrestin1/2-deficient HEK293 cells (arrestin 2/3-deficient (ΔArrb1/2) HEK293 - Clone 4) were supplied by study co-author Asuka Inoue and have been previously described.

Authentication

HEK293T/17 cells were purchased from ATCC at study initiation on 3/22/2022 and came with a supplier-provided certificate of analysis verifying authenticity. G protein-deficient and β-arrestin1/2-deficient were authenticated by PCR and SDS–PAGE and immunoblotting, as described in detail in published works. G protein-deficient HEK293 cells: Grundmann, M. et al. Lack of beta-arrestin signaling in the absence of active G proteins. Nat Commun 9, 341 (2018). https://doi.org:10.1038/s41467-017-02661-3. β-arrestin1/2-deficient HEK293 cells: O'Hayre, M. et al. Genetic evidence that beta-arrestins are dispensable for the initiation of beta(2)-adrenergic receptor signaling to ERK. Sci Signal 10 (2017). https://doi.org:10.1126/scisignal.aal3395.

Mycoplasma contamination

Cells lines tested negative for mycoplasma contamination.

Commonly misidentified lines
(See ICLAC register)

No commonly misidentified cell lines were used in this study.

Animals and other research organisms

Policy information about studies involving animals; ARRIVE guidelines recommended for reporting animal research, and Sex and Gender in Research

Laboratory animals

The mice studied in the embodied work include: C57BL/6J mice (The Jackson Laboratory, Bar Harbor, ME, Cat# 000664), global NTSR1-/- mice (B6.129P2-Ntsr1tm1Dgen/J, Deltagen, The Jackson Laboratory Strain #:005826), Beta-arrestin2-/- mice (Urs et al. (2016) Proc Natl Acad Sci U S A 113, E8178-E8186) and their wild-type littermates. Mice were 8-20 weeks old, weighed 19–30 g, and were age-matched across experimental groups. Mice were kept in a controlled room temperature environment with a 14:10-hour light/dark cycle. Humidity was maintained between 30-70%.

Wild animals

Not applicable.

Reporting on sex

Sex as a biological variable was considered. All studies included both male and female mice and treatment groups were sex-matched.

Reporting on sex	As sex-specific effects of SBI compound treatment were not identified, data from male and female mice were combined.
Field-collected samples	Not applicable.
Ethics oversight	All mouse studies were conducted in accordance with the National Institutes of Health Guidelines for Animal Care and Use of Laboratory Animals and with approved animal protocols from the University of Minnesota and Duke University Animal Care and Use Committee.

Note that full information on the approval of the study protocol must also be provided in the manuscript.

Plants

Seed stocks	*Report on the source of all seed stocks or other plant material used. If applicable, state the seed stock centre and catalogue number. If plant specimens were collected from the field, describe the collection location, date and sampling procedures.*
Novel plant genotypes	*Describe the methods by which all novel plant genotypes were produced. This includes those generated by transgenic approaches, gene editing, chemical/radiation-based mutagenesis and hybridization. For transgenic lines, describe the transformation method, the number of independent lines analyzed and the generation upon which experiments were performed. For gene-edited lines, describe the editor used, the endogenous sequence targeted for editing, the targeting guide RNA sequence (if applicable) and how the editor was applied.*
Authentication	*Describe any authentication procedures for each seed stock used or novel genotype generated. Describe any experiments used to assess the effect of a mutation and, where applicable, how potential secondary effects (e.g. second site T-DNA insertions, mosiacism, off-target gene editing) were examined.*